Characterizing Stratospheric Polar Vortex Variability With Computer Vision Techniques

Zachary D. Lawrence[1] (iD) **and Gloria L. Manney[2,1]** (iD)

[1]Department of Physics, New Mexico Institute of Mining and Technology, Socorro, NM, USA, [2]NorthWest Research Associates, Socorro, NM, USA

Abstract Computer vision techniques are used to characterize the Arctic stratospheric polar vortex in 38 years of reanalysis data. Such techniques are typically applied to analyses of digital images, but they represent powerful tools that are more widely applicable: basic techniques and considerations for geophysical applications are outlined herein. Segmentation, descriptive, and tracking algorithms are combined in the Characterization and Analysis of Vortex Evolution using Algorithms for Region Tracking (CAVE-ART) package, which was developed to comprehensively describe dynamical and geometrical evolution of polar vortices. CAVE-ART can characterize and track multiple vortex regions through time, providing an extensive suite of region, moments, and edge diagnostics for each. CAVE-ART is valuable for identifying vortex-splitting events including, but not limited to, previously cataloged vortex-split sudden stratospheric warmings. An algorithm for identifying such events detects 52 potential events between 1980 and 2017; of these, 38 are subjectively classified as distinct "split-like" events. The algorithm based on CAVE-ART is also compared with moment-based methods previously used to detect split events. Furthermore, vortex edge-averaged wind speeds from CAVE-ART are used to define extreme weak and strong polar vortex events over multiple vertical levels; this allows characterization of their occurrence frequencies and extents in time and altitude. Weak and strong events show distinct signatures in CAVE-ART diagnostics: in contrast to weak events, strong vortices are more cylindrical and pole centered, and less filamented, than the climatological state. These results from CAVE-ART exemplify the value of computer vision techniques for analysis of geophysical phenomena.

Plain Language Summary A large-scale cyclone called the stratospheric polar vortex forms in the middle atmosphere over the pole every fall in each hemisphere and lasts until spring. The Arctic and Antarctic vortices share many characteristics, including that they consist of strong eastward winds, and they extend from roughly 14 km above the surface to beyond 50 km. Understanding the behavior of these vortices is important because they affect stratospheric ozone depletion and influence weather and climate. In general, the Arctic stratospheric vortex exhibits anomalous behavior more often than its Antarctic counterpart; understanding such behavior can be aided by examining vortex geometry – their size, shape, location, etc. Here we use computer vision techniques similar to those used to analyze digital images to analyze the geometry of the Arctic polar vortex over years from 1980 to 2017. With these techniques, we find a large number of split-like events in which the Arctic polar vortex breaks apart into two separate vortices. We also find important differences in vortex geometry when the Arctic vortex is strong versus when it is weak. Our results draw attention to details of stratospheric vortex variability that motivate further investigation of the physics that can help scientists better understand middle atmosphere weather and climate.

1. Introduction

The stratospheric polar vortices that form over the Earth's poles during the respective hemispheric autumn seasons are the principal features of the wintertime stratospheric circulation. The Arctic and Antarctic stratospheric vortices share many characteristics: The edges of these vortices are delimited by intense westerly winds, which act as strong barriers that isolate the vortex interiors from midlatitude air (e.g., Manney et al., 1994; Schoeberl et al., 1992). This isolation, and the position of the vortices within the darkness of the Northern/Southern Hemisphere (NH/SH) polar night, typically allows the large pools of air within the vortices

to cool to very low temperatures (quite often below 195 K in the lower stratosphere). These characteristics of the stratospheric vortices make them critical for enabling chemical processes that allow stratospheric ozone depletion to occur (e.g., Solomon, 1999; World Meteorological Organization (WMO), 2015, and references therein).

The Arctic polar vortex tends to be smaller, warmer, and more variable than its Antarctic counterpart, largely because of hemispheric differences in orography and land-sea contrasts that lead to the generation of more planetary waves in the NH (e.g., Andrews, 1989); these waves in turn disturb the Arctic polar vortex and can reduce the strength of its edge as a transport barrier (e.g., Andrews, 1989; McIntyre & Palmer, 1983). Variability in the Arctic polar vortex is important for determining polar chemical processing and Arctic ozone depletion (e.g., Manney et al., 2011, 2015; WMO, 2015, and references therein) and is linked to surface weather and climate (e.g., Baldwin & Dunkerton, 2001; Mitchell et al., 2013), as well as to improved tropospheric predictability in forecasts (e.g., Sigmond et al., 2013; Tripathi, Charlton-Perez, et al., 2015; Tripathi, Baldwin, et al., 2015). As a result, an enormous body of research has been dedicated to understanding and characterizing the often surprising behavior of the Arctic polar vortex.

The wide spectrum of variability shown by the Arctic winter stratosphere and polar vortex has been the subject of many studies that focus on its extremes (e.g., Dunn-Sigouin & Shaw, 2015; Runde et al., 2016, and references therein). On one end of the spectrum are sudden stratospheric warmings (SSW), which are events associated with enhanced planetary wave activity in the stratosphere (e.g. Limpasuvan et al., 2004) that are eponymously named for their sudden large increases in polar stratospheric temperatures and notable for their rapid decelerations of the typically westerly zonal flow. SSWs are commonly subsetted according to their disturbance to the polar vortex, which includes displacements and splits; in the former case, the vortex ends up displaced far off the pole, while in the latter it splits into two or more offspring vortices (e.g., Charlton and Polvani, 2007, and references therein). While the mechanisms for development of SSWs are still not fully understood (e.g., Birner & Albers, 2017, and references therein), the large disturbances from SSWs have been shown to gradually descend into the troposphere over weeks to months, and they can significantly affect surface weather and climate (e.g., Baldwin & Dunkerton, 2001; Kuroda, 2008; Limpasuvan et al., 2004). The other end of the spectrum includes so-called vortex intensification events, which have been associated with decreased planetary wave driving and negative poleward heat fluxes (e.g., Dunn-Sigouin & Shaw, 2015; Limpasuvan et al., 2005; Shaw & Perlwitz, 2014). These processes can allow the vortex to strengthen via dynamical and radiative effects, which can lead to a more robust and pole-centered vortex. A lack of disturbance to the wintertime vortex and stratosphere can also give rise to signatures (opposite in sign to those from SSWs) that descend into the troposphere (e.g., Baldwin & Dunkerton, 2001; Kuroda, 2008; Limpasuvan et al., 2005).

Polar vortices are commonly described using potential vorticity (PV) data on isentropic surfaces, which acts in a similar manner to a material tracer (Hoskins et al., 1985; McIntyre & Palmer, 1984). Maps of wintertime stratospheric PV typically show the polar vortex as a roughly circumpolar cap of high-magnitude PV surrounded by low-magnitude PV values. The low-magnitude PV region around the vortex has been called the surf zone, as it is the primary region where planetary wave breaking occurs (McIntyre & Palmer, 1983). A transitional region of strong PV gradients demarking the vortex edge separates the vortex interior and surf zone (e.g., McIntyre & Palmer, 1983; Nash et al., 1996). Disturbances (or lack thereof) to polar vortices are reflected in changes (or lack thereof) in their structure; as a result, the geometry of polar vortices can be exploited to better understand the overall dynamical state of the vortex and stratosphere.

The geometrical structure of polar vortices has been widely studied because of these dynamical connections: Butchart and Remsberg (1986) found that the area of the NH stratospheric polar vortex changed in response to irreversible processes related to radiative effects and mixing and that the area diagnostic as applied to long-lived trace gases responded in a similar manner to the erosion of vortex PV via mixing. Baldwin and Holton (1988) supported this finding and further discussed how the area of the NH polar vortex is significantly affected by planetary wave breaking and could be used to diagnose a "preconditioned" state of the polar vortex in the weeks prior to SSWs. Earlier studies also highlighted the potential importance of the size and shape of the vortex as being key to understanding the preconditioning and triggering of SSWs (e.g., McIntyre, 1982; McIntyre & Palmer, 1983). These ideas and findings are still relevant; more recently, Albers and Birner (2014) suggested that there should be two separate definitions for vortex preconditioning that are indicative of vortex geometries that support triggering split versus displacement SSWs.

The vortex area diagnostic is the zeroth-order spatial moment of the vortex as represented by a contour demarking the vortex edge. Waugh (1997) and Waugh and Randel (1999) expanded the analysis of polar vortex geometry by using higher-order two-dimensional (2-D) spatial moments or elliptical diagnostics to quantify climatological differences between the Arctic and Antarctic polar vortices and to identify large-scale Rossby wave breaking events. Matthewman et al. (2009) used elliptical diagnostics to investigate the evolution and vertical structure of the polar vortex during SSWs and noted that vortex splits tend to occur nearly simultaneously throughout the stratosphere while vortex displacements tend to tilt with height. Mitchell et al. (2011) used extreme value theory and 2-D moment diagnostics to characterize Arctic and Antarctic polar vortices and showed that moment diagnostics were a useful measure of vortex variability and could be used to help distinguish vortex-split/displacement SSWs. Many studies of the polar vortex, stratospheric variability, and their connections have since made extensive use of geometric and moment diagnostics for studies based on modeling (e.g., Liu and Scott, 2015; Matthewman & Esler, 2011), reanalyses (e.g., Hannachi et al., 2011; Mitchell et al., 2013; Seviour et al., 2013), and climate model data (e.g., Maycock & Hitchcock, 2015; Seviour et al., 2017; Zhang et al., 2016)

Since stratospheric polar vortices are easily defined in dynamical fields and because their geometry provides insight into their dynamics, computer vision techniques are ideal for analyzing their behavior. The field of computer vision has sought to develop algorithms by which computers can perform tasks that the human eye does naturally. Such algorithms are typically applied to digital images for tasks including identifying objects, extracting their features, and tracking them through time. Wintertime stratospheric PV data share many characteristics of digital images that can be easily analyzed by computer vision and image processing techniques. The high PV vortex interior is well separated from the low PV vortex exterior, making the polar vortex easily distinguishable in a "scene." The shape of the vortex can also vary from elliptical to filamented and convex to concave; such features can be extracted by analyzing the vortex edge. When the vortex splits into multiple offspring or sheds filaments, the resulting separate vortex regions with differing properties can be tracked through space and time. Leveraging such techniques allows for a vortex-centered perspective that can provide unique insights into dynamics beyond that obtained from the typical zonal mean and equivalent latitude perspectives, which are views that become especially inadequate when the vortex is highly disturbed and distorted.

Our goals in this paper are twofold: first, to show how we have used computer vision techniques to analyze Arctic stratospheric polar vortex variability and second, to demonstrate the value and ease of use of such techniques for geophysical applications. To this end, the results we present include the detection and classification of "split-like" vortex events, which shows that the Arctic polar vortex exhibits split-like behavior much more frequently than vortex-split SSWs. We also show a new vortex strength definition that emphasizes differences in vortex characteristics between strong and weak states, highlights variability among major SSW events, and hints at connections between strong and weak states of the vortex.

The remainder of the paper is organized as follows: Section 2 gives some background on several basic computer vision concepts and tasks used herein. Section 3 outlines the data we use and how we apply the concepts described in Section 2 to the polar vortex. Section 4 shows our results. And section 5 summarizes our conclusions and discusses some potential future research.

2. Methods Background

Computer vision and image processing techniques are usually applied to digital images that may evolve with time. Digital images are typically treated as two-dimensional arrays of pixels that can be displayed visually, but more generally, digital images are simply data sets consisting of digitized visual information such as color or grayscale intensity. The locations of individual pixels in a digital image generally do not need to be stored as part of the data set because, in essence, the positions of individual pixels in memory describe their visual location on a grid. It is thus no surprise that computer vision and image processing techniques are more generally applicable to gridded data sets that represent other digitized information. Indeed, their application to geophysical data sets is not new: Hodges (1994) described many of the techniques that will be discussed herein and demonstrated how these techniques could be used to detect and track cyclonic activity in tropospheric relative vorticity data. Limbach et al. (2012) described an algorithm based on computer vision techniques to perform spatiotemporal (i.e., 4-D) detection and tracking of atmospheric features;

they demonstrated their algorithm by applying it to wind data to describe jet stream features and events such as jet splits and merges.

In the subsections to follow, we describe some basic computer vision concepts, terminology, and techniques. Many general resources are available that discuss computer vision and image processing (e.g., Nixon and Aguado, 2012), including detailed descriptions in Hodges (1994) and Limbach et al. (2012) for applications to atmospheric phenomena; we thus describe these concepts only at a high level and provide resources and references where possible. Readers interested only in the specific applications to the Arctic stratospheric polar vortex may skip to section 3.

2.1. Logically Rectangular Grids and Connectivity

Two important and related considerations for using computer vision techniques are the reliance on having data on a logically rectangular grid and the notion of connectivity between grid points. A logically rectangular grid is simply any grid for which a discretization of grid points maps one-to-one to indices in an index space. Such grids are not required to be orthogonal or regular, but they commonly are both. With images this is obviously the case, since the columns and rows of pixels always map to the same cartesian (x, y) coordinates. However, logically rectangular grids do not require a Cartesian coordinate system. Curvilinear coordinate systems can be logically rectangular, and indeed, these are ubiquitous in the atmospheric and climate sciences, where data assimilation systems, reanalyses, and climate models typically output quantities on regular latitude-longitude grids that span the surface of the Earth.

The connectivity of grid points in a data set must also be considered in order to identify "objects." In general, grid points are considered to be connected to their immediately adjacent neighbors. Hence, an object in a data set can be broadly defined as any set of grid points consisting entirely of adjacent neighbors that all meet some logical condition. This imposes a constraint on the logically rectangular grids to which many computer vision techniques can be applied, since many of the techniques rely on neighbors being adjacent in both "physical" and index space. For 2-D grids, the most common connectivity criteria are 4 and 8 connectivity: any given grid point is 4 connected to the grid points in index space that iterate by one in only one of the dimensions (e.g., $(i \pm 1, j)$ or $(i, j \pm 1)$), whereas a grid point is 8 connected to the grid points in index space that iterate by one in one or both of the dimensions (e.g., $(i \pm 1, j \pm 1)$). Clearly, these connectivity criteria also have analogs for n-dimensional grids.

An important intersection of these two concepts arises when considering a grid having periodic boundary conditions, such as regular latitude-longitude grids. Logically rectangular grids can be periodic, but their storage in computer memory imposes artificial boundaries at the "endpoints" of the periodic dimension(s). Thus, periodic boundary conditions must be handled explicitly, and the grid point connectivity describes how points are associated across the artificial boundaries. Awareness of this issue is important because, to our knowledge, none of the standard computer vision and image processing algorithms provided by scientific computing languages (e.g., MATLAB and IDL) and libraries (e.g., OpenCV and scikit-image) handle periodic boundaries, and hence, this responsibility falls to the user (see, e.g., Appendix A in Dias et al., 2012).

2.2. Segmentation of Objects

In computer vision, segmentation is the process of detecting individual regions within an image and highlighting them so that they are separable from each other and from other parts of the image. Segmentation can be done whether or not the specific objects to be segmented are known beforehand. When they are known beforehand, segmentation amounts to locating and labeling any and all regions that satisfy some logical condition such as finding all landmasses with surface temperatures greater than 38°C. When they are not, an image can still be partitioned into separate objects such that any individual object is "homogeneous" but "significantly different" from other objects; a simple example is classifying climate zones based on climatological surface temperature and precipitation data. In such cases, the definitions of homogeneous but significantly different will vary depending on the segmentation method used since different methods will use different criteria to determine how grid points or pixels should be grouped together. Haralick and Shapiro (1985) and Pal and Pal (1993) provide reviews of different segmentation techniques.

Objects to be segmented in a data set are often defined by the user, so the homogeneity criterion is known beforehand. In these cases, segmentation techniques work on a binarized version of the image or data, where ones/zeros indicate points that are/are not part of an object. Producing a binarized image is called thresholding because it highlights points that meet or exceed some given threshold(s). In such cases,

segmentation amounts to labeling all the separated blobs of connected ones in the binarized image. Hodges (1994) described a method for segmenting binarized images that uses a quadtree data structure (a method described generally by Horowitz and Pavlidis, 1976; Samet, 1981), which recursively divides up an image into blocks that are selectively stored as nodes in the quadtree and labels blobs by traversing those nodes of the tree. Flood filling is a technique that is conceptually simpler and easier to implement (e.g., Geraets et al., 2004; Pavlidis, 1982) that can handle periodic boundary conditions with relatively trivial modifications. Functions provided in scientific computing packages for segmentation labeling (e.g., "label_region" in IDL, "bwlabel" in MATLAB, and "skimage.measure.label" in the scikit-image python module) can be forced to handle periodic boundary conditions (with a small hit to performance) by first applying the labeling function before merging and relabeling objects that cross the periodic boundaries (based on the connectivity described previously).

2.3. Object Descriptors

Once objects have been identified, it is often desirable to calculate descriptors that provide additional quantitative information about each one. Ideally these characteristics would have desirable properties such as invariance to scale and/or translation such that the descriptors would stay approximately equal if calculated from a different scene containing a subset of the same objects (e.g., regardless of a digital photograph being taken when more/less zoomed in or from two or more different locations). The descriptors that are probably most commonly used describe the geometry of objects via their moments. In the continuous case of a 2-D region D over which a function $f(x, y)$ is defined, moments of order $i + j$ can be calculated from

$$m_{i,j} = \iint_D x^i y^j f(x, y) \, dx \, dy \tag{1}$$

With images or gridded data sets, the calculation of moments can be forced to be purely geometrical (if $f(x, y) = 1$ everywhere in D). The moments of an object can provide quantities such as centroids, orientations (the angle of the object with respect to an axis), and aspect ratios. Moments can further be used to define invariants with respect to translation, scale, and rotation called Hu moment invariants (after Hu, 1962). Many studies have used moments analyses to investigate vortex geometry (e.g., Matthewman et al., 2009; Mitchell et al., 2011; Waugh & Randel, 1999). For such applications outside of image processing, it is important to remember that the calculation of moments is sensitive to grid sampling and cell sizes; for example, latitude/longitude grids on the sphere have denser sampling near the poles where the cells decrease in area. It is common in these cases to interpolate to an appropriate Cartesian projection with regular grid spacing before calculating the moments and derived quantities and to transform back to the original coordinates (if necessary).

Retaining the boundary of an object region allows one to have access to most of the geometrical information about the object region without having to keep or process the interior points; in this sense, using boundary points offers a useful data reduction that can decrease the time and storage needed for some computations. It is usually best to have the points be ordered such that the boundary can be traversed in a clockwise or counterclockwise sense. Doing so provides extra flexibility and allows additional object descriptors such as the perimeter to be calculated. Many boundary tracing algorithms exist, including ones that are easy to implement and adapt for periodic boundaries such as the Moore-neighbor tracing algorithm (e.g., Freeman, 1970) and the Marching Squares algorithm (the 2-D analog of the 3-D Marching Cubes algorithm described by Lorensen & Cline, 1987).

Mehtre et al. (1997) and Nixon and Aguado (2012) provide more information about object descriptors.

2.4. Object Tracking

To track specific objects through time, it is beneficial to have frequent enough time sampling that objects do not move or change much between consecutive time steps. If the time sampling is dense enough that object regions are nearly stationary between time steps, then tracking can be done using spatial overlap between time steps. If the objects' descriptors stay nearly invariant between time steps, then these descriptors can also be used to track an object by matching objects that are the most similar between time steps. A combination of these two strategies can also be used.

If neither of these assumptions hold, then tracking objects requires some prediction. Reinders et al. (1999) describe a method based on "correspondence functions" that assumes that all objects evolve smoothly with time such that object descriptors (e.g., shape, size, and location) can only change within a certain tolerance.

Muelder and Ma (2009) describe a predictor-corrector tracking method that iteratively predicts the trajectory of an object based on its location at previous time steps and then corrects itself using the spatial overlap of the prediction and the real data at the next time step.

Tracking techniques have been used before for atmospheric applications: Arnaud et al. (1992) describe a method for tracking clouds in infrared images that is based on overlapping regions of clouds between time steps of successive images. Hodges (1995) developed a tracking scheme for the unit sphere based on interpolation and minimizing a cost function to follow an object through time. Hodges (1999) outlines improvements to this method that use adaptive constraints to make the tracking more flexible and accurate. Dias et al. (2012) used 3-D grid point connectivity in latitude, longitude, and time to track contiguous cloud regions and used a Radon transform technique to determine whether they propagated zonally. Souders et al. (2014a, 2014b) used techniques similar to those described by Arnaud et al. (1992) and Hodges (1999) to track Rossby wave packets defined using wind and geopotential height data.

3. Data and Methods

3.1. MERRA-2 Reanalysis

We use data from the National Aeronautics and Space Administration's (NASA) Global Modeling and Assimilation Office (GMAO) Modern Era Retrospective-analysis for Research and Applications version 2 (MERRA-2) data set (Gelaro et al., 2017). MERRA-2 uses the Goddard Earth Observing System version 5.12.4 assimilation system with incremental analysis update (Bloom et al., 1996) and a cubed sphere model for its analyses. MERRA-2 covers the satellite era from 1980 to the present and contains many upgrades over its predecessor, MERRA; these include new assimilated input data, model constraints, and parameterizations (Gelaro et al., 2017, and references therein). We use fields from the "M2I3NVASM" file collection (Global Modeling and Assimilation Office, 2015), which provides fields every 3 h on a 0.625° × 0.5° longitude/latitude grid with 72 hybrid σ pressure levels ranging from the surface to 0.01 hPa.

3.2. CAVE-ART

Here we present the "Characterization and Analysis of Vortex Evolution using Algorithms for Region Tracking" (CAVE-ART) package that was developed to comprehensively describe the state of the winter stratospheric polar vortex. CAVE-ART makes extensive use of the computer vision techniques described in section 2.

CAVE-ART uses PV data on isentropic surfaces to define the stratospheric polar vortex. We scale the PV used by CAVE-ART into vorticity units as in Dunkerton and Delisi (1986) by dividing by a standard static stability derived from assuming a constant lapse rate of 1 K km^{-1} and a pressure of 54 hPa on the 500 K isentropic level; this is done so the values of scaled PV (hereinafter referred to as sPV) are of the same order of magnitude throughout the stratosphere. Other inputs to CAVE-ART include temperature, geopotential height, and zonal and meridional wind components. For all the results shown herein, all of these fields are vertically interpolated from MERRA-2 model level data to 21 isentropic surfaces ranging from 410 K in the lowermost stratosphere (LMS) to 1500 K in the upper stratosphere.

CAVE-ART treats the meteorological fields as digital images with cylindrical periodicity (i.e., periodicity only in longitude). The stratospheric polar vortex is the object of interest that CAVE-ART segments, characterizes, and tracks through time; using sPV, the stratospheric vortex is defined on individual isentropic levels as the objects having sPV larger than the vortex edge values of sPV. To define the vortex edge, we use a climatological profile of vortex edge values derived from MERRA-2 data over all NH winters from 1979/1980 to 2015/2016 (see section 3.3). Finally, to allow for the most accurate tracking possible, we use meteorological data for all 8 times per day provided by MERRA-2.

Figure 1 shows (for a single day and level) the following steps that CAVE-ART performs after the data have been read and interpolated to isentropic surfaces:

1. The sPV data are binarized using the vortex edges on each isentropic surface.
2. Flood filling is used to segment each closed contour of sPV on each isentropic surface.
3. Areas are calculated for each potential vortex object; those with areas below a specified threshold are filtered out.
4. Ordered boundary points are derived for every remaining vortex object using a Marching Squares algorithm.
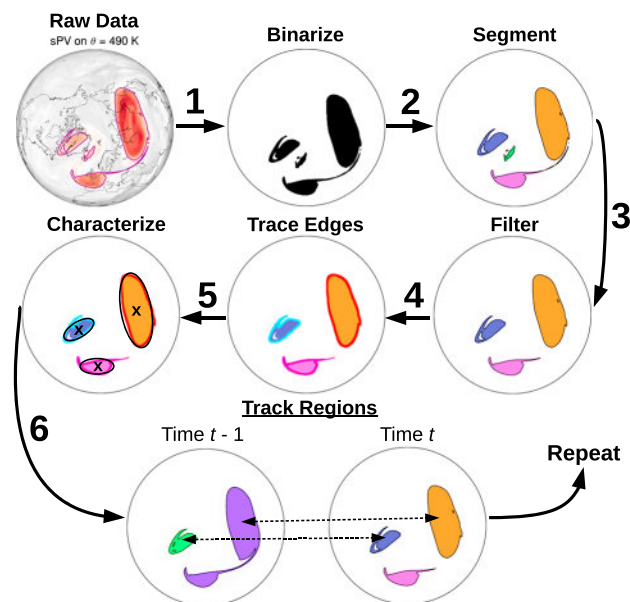
Figure 1. Schematic of the steps that CAVE-ART goes through to characterize and track polar vortex regions.

5. Diagnostics are calculated for each individual vortex object; these diagnostics include some from a moment analysis.
6. The predictor-corrector tracking algorithm of Muelder and Ma (2009) is used to track the vortex objects through time to match the regions remaining after the segmentation and filtering (steps 2 – 3).

All of the algorithms used in steps 2, 4, and 6 were adapted to handle the periodicity in longitude. In step 3, we calculate the areas of the potential vortex objects in spherical coordinates and filter using an equivalent latitude threshold of 85°. Thus, if an individual vortex object were mapped to a polar cap having equivalent area, it would be filtered out if the boundary of that polar cap is poleward of 85°; this corresponds to an area less than roughly 0.4% of a hemisphere. This threshold was chosen to eliminate the influence of small vortex filaments, as well as isolated regions of elevated PV that sometimes arise in the lower stratosphere in reanalysis fields. In many cases the region tracking of step 6 is unnecessary simply because the vortex does not split very often. However, when it does split, the overlap assumption in our predictor-corrector algorithm is usually suitable for data sampled at 4 or more times per day. Small regions such as narrow filaments sometimes do not overlap between time steps, and thus, these can require multiple time steps to predict their trajectories.

CAVE-ART provides three categories of diagnostics: moment diagnostics, region diagnostics, and edge diagnostics. The moment diagnostics include centroids, aspect ratios, angles, and excess kurtosis (see Matthewman et al., 2009, for more details). The region diagnostics include vortex area, area-weighted averages of vortex temperatures, altitudes, and sPV, minima and maxima in vortex temperatures and altitudes, the value and location of the maximum vortex sPV, and a couple of polar processing diagnostics (calculated only for isentropic levels below 750 K) including sunlit vortex area and concentricity of the vortex with cold regions having temperatures below polar stratospheric cloud thresholds (see Lawrence et al., 2015, for more details). The vortex edge diagnostics include edge-averaged horizontal sPV gradients, edge-averaged wind speeds, circulation, and vortex edge length.

To construct climatologies of diagnostics that are inherently calculated for multiple regions, we postprocess the CAVE-ART data to compact the diagnostics in a few ways: Extensive properties of the vortex (vortex area and edge length) are simply summed across all individual regions. Dynamical properties of the vortex are collapsed into single values by taking area-weighted averages of all individual regions; thus, under normal conditions, small regions and filaments will minimally affect a large and coherent main vortex, whereas during a split, individual offspring vortices will contribute in proportion to their relative sizes. Moment diagnostics are calculated within CAVE-ART for individual regions as well as for the bulk filtered PV fields; thus, any time a single representative moment value of the vortex is needed, we use the moment diagnostics calculated from the PV fields that have only had small high PV regions filtered out.

3.3. Vortex Edge Definition
It is often necessary to define the stratospheric polar vortex edge. Strategies for identifying the vortex edge have been around for a while (e.g., Dameris et al., 1995; Manney et al., 1994; Nash et al., 1996; Paparella et al., 1997; Rummukainen et al., 1994; Trounday et al., 1995; Waugh, 1997; Waugh & Randel, 1999). Typically, these methods either use daily values of PV, constant values of PV, or even PV at a constant equivalent latitude. We opt for using climatological constant PV values (defined below) to define the vortex edge in CAVE-ART. Although a specific PV contour cannot be expected to remain the vortex edge over time because of nonconservative processes (e.g., Butchart & Remsberg, 1986; McIntyre & Palmer, 1984; Nash et al., 1996), the vortex edge region is defined by steep horizontal gradients in PV. Hence, as noted in previous studies (e.g., Manney et al., 2007; Waugh & Randel, 1999), there will always exist a range of PV values at any given time that would accurately represent the shape, size, and evolution of the polar vortex about as well as a time-varying value. Previous studies in which we used constant vortex edge values (Manney & Lawrence, 2016; Manney et al., 2015) showed that long-lived stratospheric tracers such as N_2O and CO closely follow these constant edge values. In addition, previous studies have also pointed out some issues with automated daily vortex edge
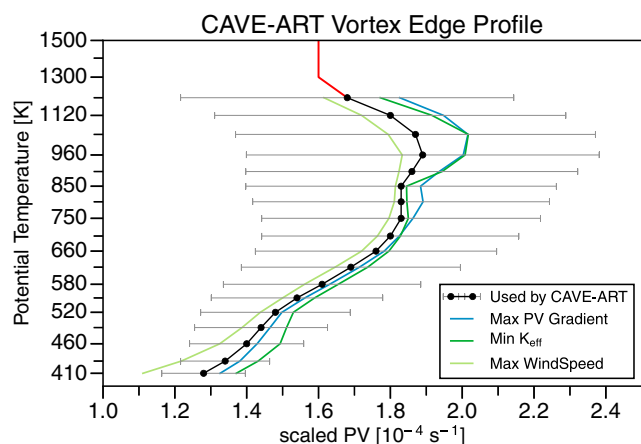
Figure 2. Vertical profiles of vortex edge-scaled potential vorticity values. The green and blue solid lines indicate the vortex edge values determined from the individual diagnostics indicated in the legend, while the black line indicates the edge values used in CAVE-ART to define the Arctic polar vortex. The error bars on the profile used by CAVE-ART represent the climatological 1 standard deviation envelopes. The red portion of the profile between 1300 and 1500 K is where we specify a constant value to define the vortex edge (see main text).

identification, especially in the upper stratosphere and mesosphere when the vortex is weak or disturbed (e.g., Harvey et al., 2009; Manney et al., 2007, and references therein).

To define our constant vortex edge values, we use the extreme values in equivalent latitude profiles of PV gradients (PVG), wind speeds (WS), and effective diffusivity (K_{eff}; calculated as in Nakamura & Ma, 1997). K_{eff} measures the complexity of tracer contours (here based on PV) to diagnose transport barriers; low (high) values in K_{eff} indicate low (high) complexity and thus weak (strong) mixing (e.g., Allen & Nakamura, 2001; Haynes & Shuckburgh, 2000; Nakamura, 1996). Minima in K_{eff} can thus be used to identify the transport barrier at the vortex edge, similarly to maxima in PVG and WS. However, the extrema of these diagnostics do not always align perfectly. We thus scale PVG and WS to the range 0–1 and K_{eff} such that its minima become maxima (and vice versa) in the range 0–1. We then define the vortex edge on a given day as the PV value at the equivalent latitude of the maximum product of the scaled versions of K_{eff}, PVG, and WS; this product is guaranteed to be less than or equal to 1 depending on how well the extrema in each of the diagnostics align with each other. This process was repeated for all days in the 1979/1980–2015/2016 climatology on individual isentropic levels between 410 and 1500 K. We include days from October to May to ensure that we capture the development and breakup of the vortex. This introduces a lot of seasonal and interannual variability, and thus, the edge values obtained tend to be on the low end of the range of the vortex edge region during the height of the winter season. However, this is helpful since it facilitates capturing the geometry and dynamics of the vortex during highly disturbed conditions.

Figure 2 shows the profile of vortex edge values we use in CAVE-ART (with climatological one standard deviation error bars) defined as described above, as well as profiles of the climatological edge values that would be obtained from using any of the WS, K_{eff}, or PVG diagnostics alone. At 1300, 1400, and 1500 K (red line in Figure 2), we encountered issues with determining the vortex edge based on any combination of PVG, WS, and/or K_{eff}. Similar issues have been noted previously since equivalent latitude becomes less appropriate as a vortex-centered coordinate in the upper stratosphere (e.g., Harvey et al., 2009; Manney et al., 2007). Thus, we chose constant sPV values of 1.6×10^{-4} s^{-1} based on visual inspection of many PV maps in this region. Below these levels, Figure 2 shows that in a climatological sense, the vortex edge values are not very sensitive to the choice of diagnostic used; however, the combined approach we use does pick a smoother profile that varies less dramatically between levels, particularly at the lowest levels from 410 to 460 K and the highest levels from 850 to 1200 K.

4. Applications and Results

Many of the algorithms and diagnostics described in section 3 have been used before for studies involving the polar vortex. Manney et al. (2015) used an early version of CAVE-ART on the 2012/2013 vortex-split SSW to examine how the unique dynamical conditions within the vortex before and during the split contributed to rapid early winter ozone loss. These computer vision techniques allowed us to examine trace gas and temperature distributions in the individual offspring vortices throughout the entire vortex-split event. More recently, Manney and Lawrence (2016) used CAVE-ART to examine the "major final warming" of the NH polar vortex in 2016. As part of our analysis, segmentation of the vortex fragments and offspring during the vortex breakdown allowed us to examine parcel trajectories initialized within specific pieces of the vortex, which showed the rapidity of the vortex breakdown and the dispersal of vortex air. The segmentation and tracking methods used in CAVE-ART are uniquely suited to this type of comprehensive characterization of multiple vortex regions. In the following subsections we discuss additional applications of the diagnostic products provided by CAVE-ART. The results we show below cover all Arctic winters from 1979/1980 to 2016/2017.

4.1. Vortex-Split Events

One strength of CAVE-ART is its inherent ability to directly detect vortex-split events; rather than relying on any underlying dynamics or definitions, it simply uses computer vision methods to detect and track materially
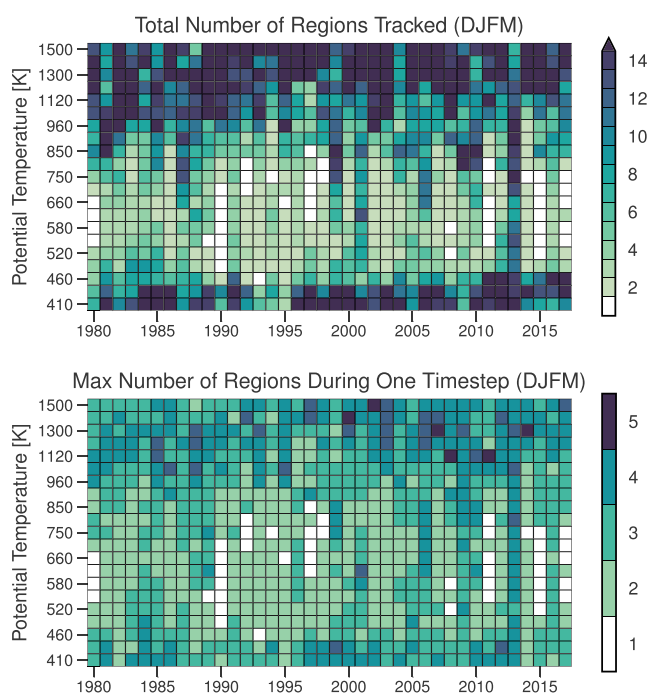
Figure 3. Matrix plots showing the (top) total number of regions tracked by CAVE-ART and (bottom) the maximum number of regions detected by CAVE-ART at one time step for each isentropic level over all DJFM seasons in MERRA-2.

separated contours of PV. This capability does not seem to be entirely new: Waugh and Randel (1999) mention "Note that occasionally the Arctic vortex splits into two large fragments (e.g., wave 2 warmings), and although the [moment diagnostics] can be calculated for each fragment we focus here only on the larger of the fragments." Charlton and Polvani (2007) (hereinafter referred to as CP07) mention using similar methods in a footnote: "In our algorithm, contours that enclose the maximum absolute vorticity are found by considering the 8-point adjacency of grid points to the maximum absolute vorticity, making binary images of these grid points and then contouring the binary images." CP07 further state that, as part of their algorithm, they compute the number of closed contours equal to the vortex edge value (in absolute vorticity). To our knowledge, however, these sorts of methods have not been applied systematically before.

Figure 3 summarizes the region detection and tracking capabilities of CAVE-ART; it shows matrix plots of the total number of regions tracked by CAVE-ART having a lifetime of 1 day or longer over the DJFM seasons in MERRA-2 (top) and the maximum number of regions that exist at any given time step during DJFM (bottom). Figure 3 shows that CAVE-ART commonly tracks more than two regions during any given winter. Especially in the LMS where the subvortex is less well defined and in the middle to upper stratosphere where the surf zone is particularly vigorous, many of the regions tracked are due to vortex filamentation events. Thus, Figure 3 demonstrates that to detect actual vortex splits, additional diagnostics and information are necessary to distinguish them from filamentation events.

Matthewman et al. (2009) detected vortex splits during SSWs using "excess kurtosis," a moment diagnostic that takes on negative values as the underlying region of interest becomes pinched such that a separation into two or more regions is possible. They used an excess kurtosis threshold of −0.1 to diagnose the initiation of a vortex split. In a later modeling study that used moment diagnostics, Matthewman and Esler (2011) diagnosed vortex splits using an excess kurtosis threshold of −0.6. Seviour et al. (2013) similarly used a moment-based diagnostic to define vortex-split events: they used the aspect ratio of a contour of geopotential height at 10 hPa (as well as PV at 850 K) to define vortex-split events when the aspect ratio exceeded 2.4 for at least seven consecutive days.

We detect split-like events of the NH polar vortex using the diagnostics cataloged by CAVE-ART. Specifically, we search for vortex splits in DJFM by using the vortex area diagnostic on 14 isentropic levels spanning the lower and middle stratosphere from 430 K to 960 K; these level limits were chosen based on Figure 3 to correspond with the levels below and above which the number of filamentation events increase dramatically. The only requirements that we impose to define split-like events are (1) a vortex region having an area of at least 1% of a hemisphere (EqL ≈ 81.9°) must split from a vortex region that had an area of at least 2% of a hemisphere (EqL ≈ 78.5°) prior to the split and (2) the split-like event must last at least 12 h. While we did not test sensitivity to changes in these thresholds, we did intentionally choose them to be small to prevent exclusion of potentially interesting behavior. They were also chosen with knowledge that offspring vortices during some split SSWs can be rather small at some levels (e.g., around 2% of a hemisphere in the lower stratosphere of the January 2013 split; not shown) and the fact that some vortex splits can be relatively brief (see, e.g., the "vacillation-like" splits discussed in Scott, 2016), which, when using a constant vortex edge contour, could be made shorter artificially. To find the dates of split-like events, we search on all the isentropic levels between 430 and 960 K for discontinuous negative jumps in the area of the largest vortex region detected by CAVE-ART that are concurrent with CAVE-ART detecting the genesis of a new region. We then flag these onset dates if the "offspring" vortex survives for at least 12 h (satisfying condition (2) above). Finally, we pool the flagged onset dates from different isentropic levels together by grouping all onsets that occur within a 3 day window of one another (our results are not sensitive to using stricter time windows down to 1.5 days). We then consider a potential event to be detected if at least four consecutive isentropic levels have flagged onset dates pooled together (which implies a vertical coherence of the event spanning at least 120 – 200 K) and/or if at least 7 of the 14 isentropic levels are in a grouping of onset dates. Please see the Appendix A for discussion regarding the sensitivity to these level thresholds. The method as described above captures 52

Table 1

Table of Onset Dates of Split-Like Vortex Events Defined Using CAVE-ART Data

Onset of split-like events	Potentially associated major SSWs
10 Mar 1981	–
25 Jan 1982	–
15 Mar 1982	–
22 Mar 1983	–
30 Dec 1984	1 Jan 1985
20 Jan 1985	1 Jan 1985
23 Mar 1986	–
16 Dec 1987	8 Dec 1987
15 Mar 1988	14 Mar 1988
19 Feb 1989	21 Feb 1989
3 Feb 1991	–
18 Mar 1993	–
3 Jan 1994	–
14 Mar 1994	–
13 Feb 1995	–
14 Mar 1996	–
21 Jan 1998	–
8 Mar 1999	26 Feb 1999
20 Mar 2000	20 Mar 2000
16 Dec 2000	–
2 Mar 2001	11 Feb 2001
2 Dec 2001	–
25 Mar 2002	–
20 Jan 2003	18 Jan 2003
17 Feb 2003	–
5 Feb 2004	–
22 Mar 2005	–
8 Feb 2007	–
28 Jan 2009	24 Jan 2009
11 Dec 2009	–
11 Feb 2010	9 Feb 2010
6 Mar 2012	–
9 Dec 2012	–
8 Jan 2013	6 Jan 2013
15 Feb 2014	–
29 Mar 2014	–
5 Jan 2015	–
14 Mar 2016	–

Note. The second column lists Charlton and Polvani (2007) major SSW dates from MERRA-2 (as provided by Butler et al., 2017) if a split-like onset date is within a week prior to or within 20 days after a major SSW event.

events overall. We subdivide these detected events by making the final decisions as to whether they classify as split-like events by visually inspecting PV maps throughout the stratosphere in the days surrounding every event. Our final decisions are based on the geometrical evolution of the event; we specifically take into account markers of splits such as vortex elongation and pinching prior to the event, as well as the vertical coherence of the disturbance (which may not always show up as a split at some levels using the CAVE-ART vortex edges). Of the 52 events detected, we classify 38 as clear split-like events, 10 as "dubious," and 4 as false positives. The events we consider dubious are events that share some evolutionary qualities of other clear splitting events but are unclear in other ways, such as temporal proximity to other disturbances and/or unusual vortex geometry. The false positives are events that show no split-like behavior, and the four we list all arise from large vertically deep filamentation events. Our visual inspections of events included PV maps from both the MERRA-2 and ERA-Interim reanalyses; we found that vortex evolution was nearly identical in all cases from both reanalyses.

Since our visual inspection introduces subjectivity into our analysis, we include not only the list of dates of events classified as split like (Table 1) but also the dates of dubious and false positive events (Table 2). Furthermore, we include figures, notes, and reasonings for all 52 subjective classifications as a supporting information.

Figures 4 and 5 illustrate all of the split-like events listed in Table 1 with isosurface plots spanning 450 to 1000 K showing the 3-D geometry of the events and contour plots showing polar stereographic projections of the vortex edge contours at 490 and 850 K. Of the 38 split-like events, only 12 are within a week prior to, or within 20 days after, major SSWs (Figures 4e, 4f, 4h, 4i, 4j, 4r, and 4s and Figures 5b, 5e, 5j, 5l, and 5o) as defined by Charlton and Polvani (2007), with MERRA-2 onset dates from the SSW compendium (Butler et al., 2017). Furthermore, only 16 of these split-like events occur during March; while 16 of 38 is a large fraction of the events, only 7 occur after 15 March. Hu et al. (2014) found that the climatological final warming onset date in the period between 1958 and 2012 is in mid-April and that only five winters in this period had final warming onsets before 15 March. Taken together, the above results indicate that many of the 38 split-like events we show here are distinct from (but not necessarily unrelated to) both major SSWs and final warmings.

Thirty-eight events in the 38 years from 1979/1980 to 2016/2017 are many more events per year than is typically cited. The reasons for this can be understood by comparing with other methods of defining vortex-split events: Charlton and Polvani (2007) listed 15 vortex-split SSWs between 1958 and 2002 determined from subjective analysis of polar vortex evolution from two reanalyses. Their characterization of vortex disturbances is predicated on the definition of a major SSW (a zonal wind reversal at 60°N and 10 hPa) having been met; they also require that events be separated by at least 20 consecutive days of westerly winds, and in the case of split events they require that the ratios of circulations of the two offspring vortices be at least 0.5. Our algorithm using CAVE-ART data to detect potential split-like events requires no underlying dynamical conditions be met, and we apply no time-based thresholds to exclude events; we do, however, subjectively classify some events occurring within 10 days of others as dubious (see Table 2 and supporting information). Mitchell et al. (2013) identified 21 split vortex events during the same period (1958–2002), with 3 being "mixed" cases wherein the vortex changes between split and displaced states. Their events were based on diagnostics calculated using PV only at 850 K (although they mention that their results are insensitive to choice of level between 650 and 1050 K), and they require that the vortex be disturbed for five consecutive days. Our split identification requires that a split occurs across multiple isentropic levels and that an offspring vortex must persist for only 12 h or more. We also find several split-like events that are only detected in the lower stratosphere, at levels below 700 K (e.g., Figures 4c, 4o, 4p, 4q, and 4r and

Table 2
Table of Dubious Events (Denoted by D) and False-Positive Detections (Denoted by FP) Discussed in Section 4.1

Dates of dubious and false-positive detections
11 Jan 1982 - D
15 Mar 1984 - D
28 Jan 1987 - FP
15 Feb 1991 - D
27 Jan 1992 - FP
22 Mar 1994 - D
22 Dec 1998 - D
10 Jan 1999 - D
20 Feb 2001 - D
26 Jan 2003 - D
15 Mar 2005 - D
30 Jan 2006 - D
28 Feb 2008 - FP
31 Dec 2012 - FP

Figures 5c, 5g, 5k, 5m, 5q, and 5r). Seviour et al. (2013) identified 18 vortex-split events between 1958 and 2009; their split events were defined as cases where the aspect ratio of the vortex as defined in 10 hPa geopotential heights remained above 2.4 for at least 7 days, with events separated by at least 30 days. In addition to defining events using multiple vertical levels and requiring that events only last 12 h, we do not impose any constraints on the geometrical distribution of vortex PV, and we allow relatively small offspring (1% of a hemisphere in size) to be considered as valid — it is unclear how moment-based diagnostics will handle large disparities in the relative sizes of split vortices (see, e.g., Figures 4o and 4q) or cases where the vortex regions are not widely separated (see, e.g., Figures 4n, 5n, and 5p).

To compare some of our split-like events with the moment-based thresholds defined by Matthewman et al. (2009), Matthewman and Esler (2011), and Seviour et al. (2013), we show in Figure 6 time/height cross sections of the number of vortex regions seen by CAVE-ART centered on the dates of several representative events from Table 1. The overlaid cyan and magenta contours indicate the excess kurtosis and aspect ratio thresholds used to define splitting events in the previous studies. These contours are based on moments calculations derived using the full PV fields with no filtering of small regions like that done in CAVE-ART. In nearly all cases the aspect ratio and excess kurtosis thresholds are exceeded a few days prior to the split detected by CAVE-ART, which is to be expected since the vortex undergoes elongation and pinching before splitting. The aspect ratio threshold may be exceeded weeks before or after the main CAVE-ART splitting events since the vortex can become elongated without splitting. Recall that Seviour et al. (2013) also require that the aspect ratio remains above 2.4 for 7 days; the table of dates provided in the supporting information of Seviour et al. (2013) does not list the events in Figure 6a or 6e. Figure 6a may not be identified because of differences in the representation of the vortex between PV and geopotential height data that may affect the 7 day criterion; Figure 6e was likely not included because of an earlier event on 17 January 2003 that puts the event around 15 February 2003 within 30 days. The excess kurtosis diagnostic tracks the splits detected by CAVE-ART quite well in many cases (Figures 6b, 6e, 6f, 6g, and 6h), but the more stringent −0.6 excess kurtosis threshold is rarely exceeded. Because excess kurtosis is defined using second- and fourth-order moments of the PV distribution, it is much more susceptible to become positively skewed by filamentation (which can affect its ability to identify pinching) than the aspect ratio, which is why the −0.1 isolines of excess kurtosis can be vertically incoherent (e.g., as in Figures 6b and 6f) and why it may not track some events (e.g., Figures 6a, 6c, and 6d) very well. The aspect ratio and excess kurtosis can also perform well in cases that CAVE-ART nearly misses, like the 5 January 2015 event in Figure 6h.

All together, these results indicate a clear utility for moment-based diagnostics to aid in the detection of split-like vortex events. However, there could be issues in cases where the relative sizes of the split vortices are disparate enough that the parent vortex consists of a much larger fraction of the PV distribution than the offspring vortex (e.g., as in the February 1995 case shown in Figure 6c). Readers interested in using such techniques should understand the strengths and weaknesses of each one: Excess kurtosis detects pinching, but it may have issues detecting pinching when the relative sizes of the "lobes" are disparate and can be positively skewed by filamentation. The aspect ratio detects elongation, but elongation for long periods of time may not always imply a splitting event, and the vortex stretching from small split-like events may not be significant enough for it to detect anything. Further, both the aspect ratio and excess kurtosis require choosing thresholds that define what is stretched or pinched enough to be an event of interest. Segmentation methods detect material separation but can miss events if an inappropriate contour is used.

4.2. Vortex Strength

Many studies have stressed the importance of the strength of the vortex for various phenomena, including polar chemical processing (e.g., Schoeberl & Hartmann, 1991; Manney et al., 2011; Manney & Lawrence, 2016), stratosphere-troposphere coupling (e.g., Baldwin & Dunkerton, 2001; Limpasuvan et al., 2005), and improving forecasts (e.g., Thompson et al., 2002; Jung & Barkmeijer, 2006; Tripathi, Charlton-Perez, et al., 2015). Commonly used measures of vortex strength include quantities based on zonal winds (e.g., as in Limpasuvan et al., 2005; Tripathi, Charlton-Perez, et al., 2015), annular mode indices (e.g., as in Baldwin & Dunkerton, 2001),
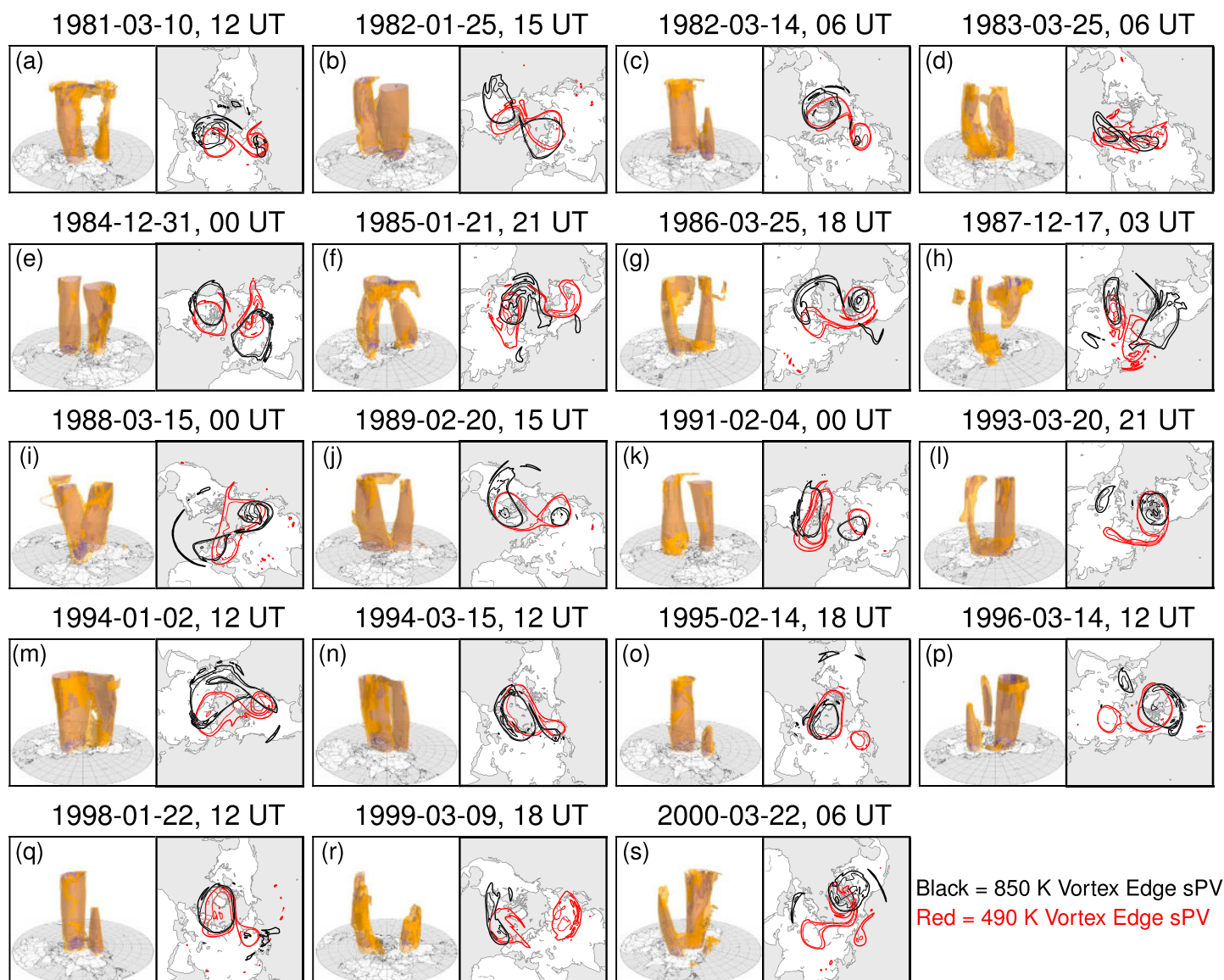
Figure 4. (a – s) Side-by-side isosurface volumes of sPV contours in the vortex edge region and polar stereographic projections of the same vortex edges for the first 19 split-like events listed in Table 1. The isosurface plots have the CAVE-ART vortex edges in orange (on the outside), as well as CAVE-ART edges plus 0.4×10^{-4} s^{-1} in dark blue (on the inside) covering isentropic levels from 450 K to 1000 K. The polar stereographic projections show the same edge contours at 490 (in red) and 850 K (in black). Note that in each case we have chosen dates that are within 3 days of the onset events listed in Table 1 and have rotated the isosurface and stereographic projections to best emphasize the vortex geometry. Also, note that the contour maps show contours of the raw sPV fields with no filtering of small regions applied.

and PV-based equivalent latitude measures (e.g., as discussed in section 3.3 and Manney & Lawrence, 2016). Herein, we use DJFM anomalies of vortex edge-averaged wind speeds to define extreme strong and weak states of the Arctic polar vortex throughout the stratosphere.

Figure 7 shows the MERRA-2 DJFM climatological seasonal cycle of vortex edge-averaged wind speeds derived from CAVE-ART. Below about 600 K, wind speeds in the vortex edge region tend to stay relatively constant throughout the DJFM season, only increasing/decreasing by roughly 5 – 10 m s^{-1} at the beginning/end of the season, respectively. Wind speeds also increase with altitude in this region by roughly 10 m s^{-1} per 100 K change in potential temperature. Above about 700 K, wind speeds in the vortex edge region show much greater seasonal variations. Vortex edge wind speeds in this region tend to be above 60 m s^{-1} from mid-December to mid-February, after which the winds decelerate by approximately 10 m s^{-1} every 2 weeks
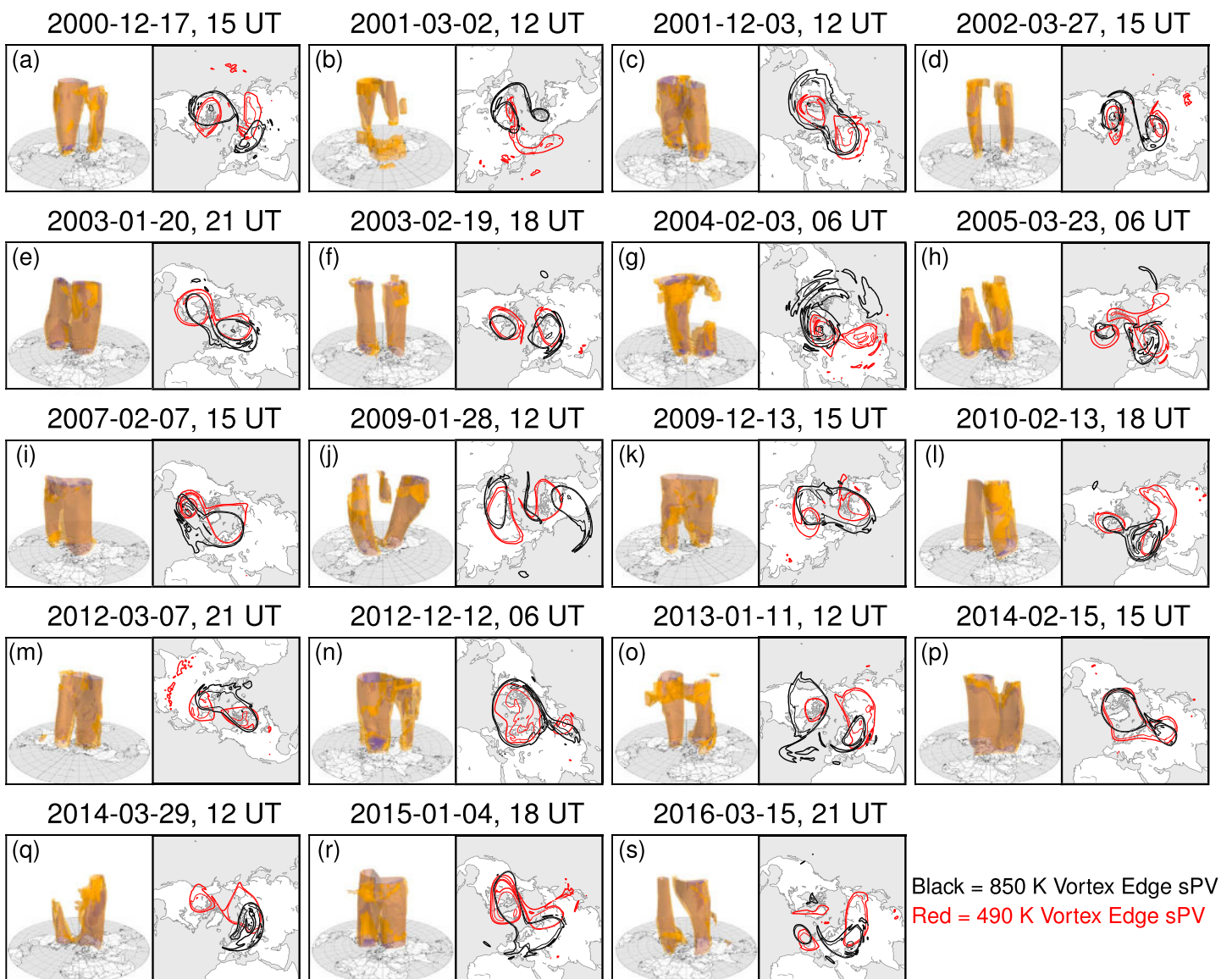
Figure 5. As in Figure 4 but for the second half of the split-like events listed in Table 1.

up until April. These patterns reflect not only the wide interannual variability in the middle stratosphere but also the short radiative timescales relative to the lower stratosphere.

Distributions of the anomalies obtained by subtracting out the above climatological seasonal cycle are used to define weak and strong vortex events. We specifically define the onset of weak/strong events on individual isentropic levels as cases when the vortex edge wind speed anomalies become more extreme than the 5th/95th climatological percentiles. We then allow these events to last until the wind speed anomalies go above/below the 10th/90th percentiles; we use relaxed percentiles for the termination of events to avoid cases in which wind speed anomalies right on the edge of the 5th/95th percentiles repeatedly oscillate above or below the extreme thresholds, allowing such cases to be considered single events rather than multiple rapid ones. Figure 8 shows some examples of standardized probability distribution functions of the vortex edge wind speed anomalies on individual levels throughout the stratosphere characterized by CAVE-ART. In the lowermost stratosphere (exemplified by 410 K), and in the upper stratosphere (exemplified by 1200 K), the distributions of wind speed anomalies are fairly Gaussian. At levels in between, the distributions tend to be skewed, with larger probabilities on the negative anomaly tails. These patterns are to be expected: In the LMS, the edge wind speeds (see Figure 7) are indicative of the wind speeds of the subvortex, which is not as well
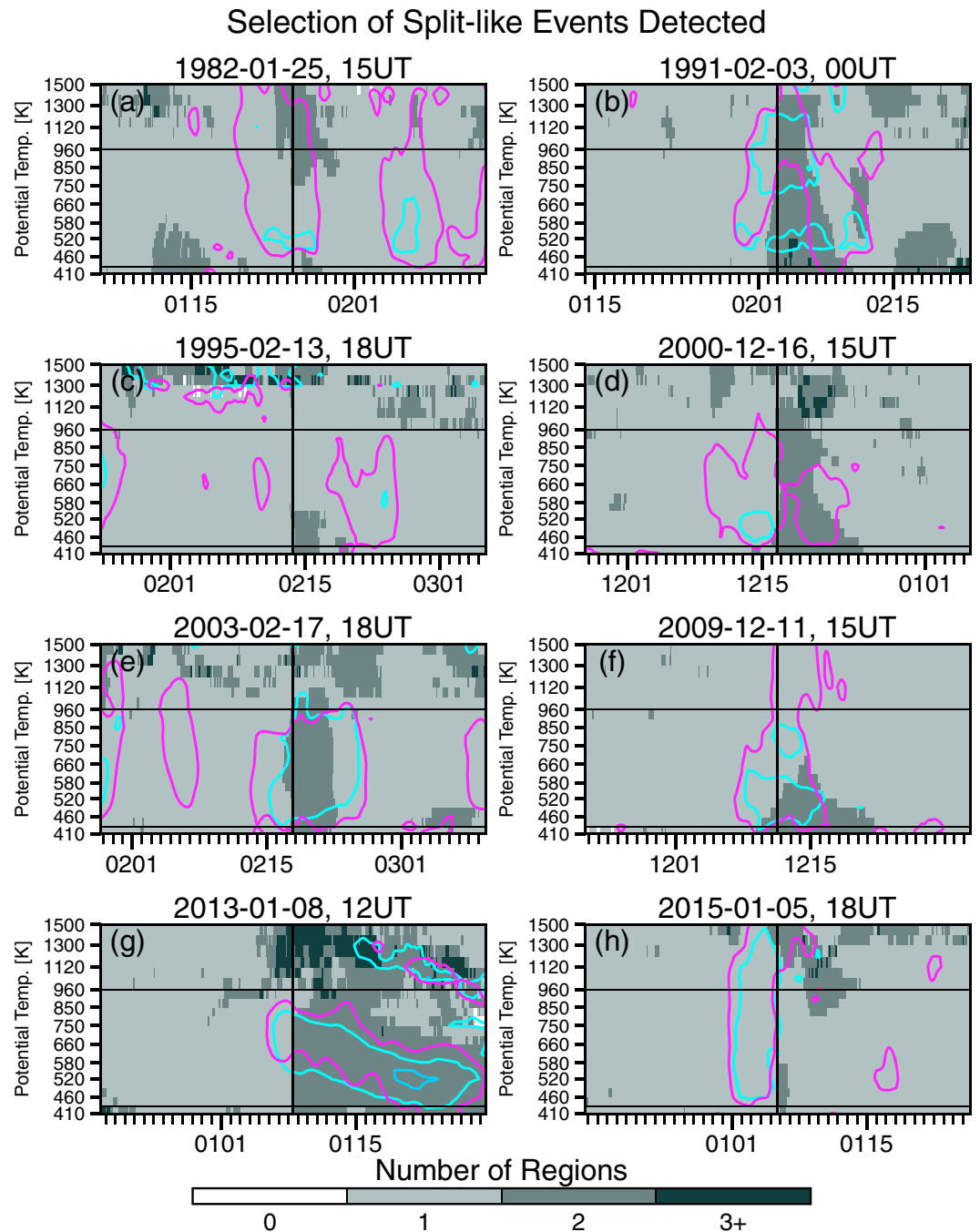
Figure 6. (a–h) Potential temperature/time cross sections showing the number of objects detected by CAVE-ART (gray scale) for a representative set of events from Table 1. The magenta and cyan/blue contours indicate the 2.4 aspect ratio and −0.1/−0.6 excess kurtosis thresholds used previously to define vortex-split events (see main text). The black horizontal lines indicate the range of levels used to define the split events in Table 1; the black vertical line shows the center of the time series as defined by the split onset dates. Dates on the *x* axes are in MMDD format, and ticks are displayed at 00 UT of each day for 20 days prior to and following the onset dates. The number of regions in the gray shades has been filtered such that only regions with areas greater than 1% of a hemisphere are included in the total.
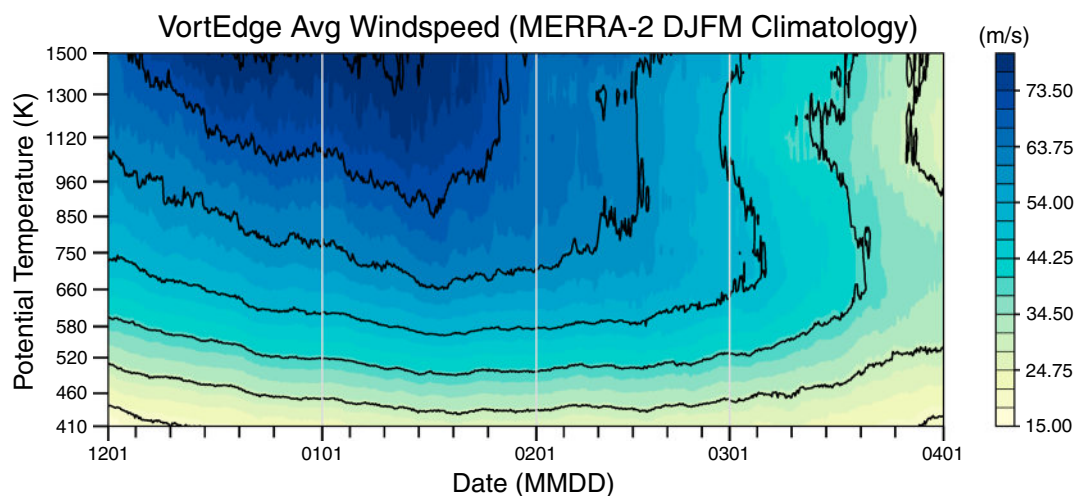
Figure 7. MERRA-2 DJFM climatology (1979/1980–2016/2017) of wind speeds averaged around the Arctic polar vortex edge derived from CAVE-ART data. The black lines are contours of wind speed ranging from 20 to 80 m s^{-1} spaced in intervals of 10 m s^{-1}.

defined as the vortex proper at higher levels (e.g., McIntyre, 1995), and hence, it is not dynamically unreasonable for wind speeds to intensify above or weaken below the climatology where the wind speeds are relatively small. Things are similar for the upper stratosphere where the combination of short radiative time scales and the very vigorous surf zone allows for the vortex to weaken or intensify symmetrically about the climatology. At the levels in between where the vortex is more well defined and robust, large disturbances from major and minor warmings can easily disturb the vortex edge wind speeds far below the climatology, but intensifications of the vortex to 2–3 σ above the climatology are unlikely from a dynamical viewpoint.

Figure 9 shows selected CAVE-ART diagnostics during winters with large weak/strong vortex events. Figures 9a, 9c, 9e, and 9g show the winter of 2012/2013 with a major SSW, while Figures 9b, 9d, 9f, and 9h show the quiescent winter of 2013/2014 that had a relatively strong vortex. The diagnostics shown include vortex edge wind speeds (Figures 9a and 9b), horizontal sPV gradients averaged around the vortex edge (Figures 9c and 9d), vortex area (Figures 9e and 9f), and the log ratio of the vortex edge length to the circumference of the vortex equivalent ellipse (Figures 9g and 9h). This last diagnostic is philosophically similar to effective diffusivity (Nakamura & Ma, 1997), except that it specifically represents the ratio of the vortex edge length to the circumference of its equivalent ellipse having equal area, angle, and aspect ratio. Hence, the log (base 2) of this ratio would be equal to 0 if the vortex edge length matched the circumference of its equivalent ellipse; values greater than 0 thus indicate a geometric deviation from a "perfect" ellipse, and the diagnostic thus acts as a measure of geometric disturbance and filamentation. Figure 9 shows that during the weak vortex
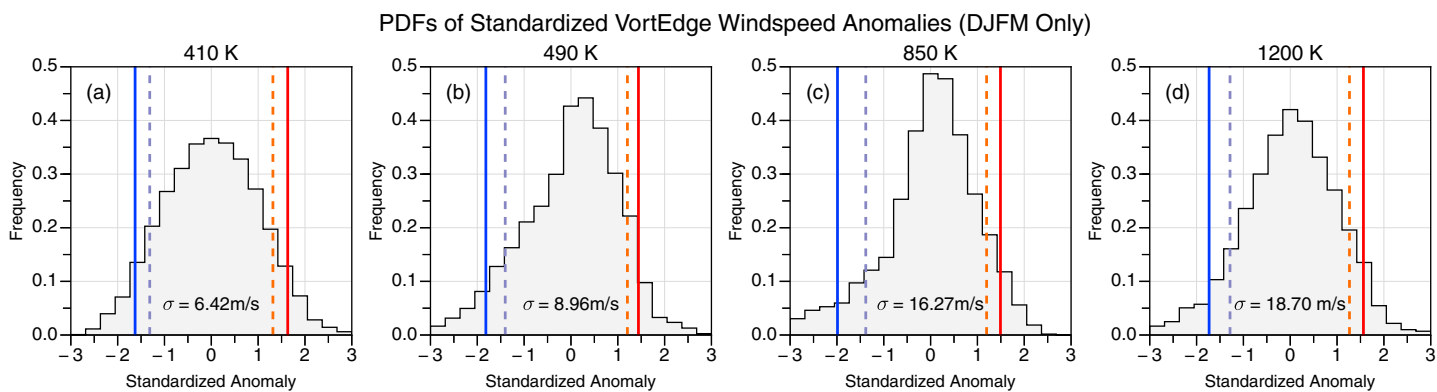

Figure 8. Standardized probability distribution functions of DJFM Arctic vortex edge wind speed anomalies in the stratosphere at (a) 410, (b) 490, (c) 850, and (d) 1200 K. The blue/red solid vertical lines indicate the 5th/95th percentiles of the distributions used to define the onset of weak/strong vortex events; the dashed purple/orange lines indicate the 10th/90th percentiles used to define the end of weak/strong vortex events.
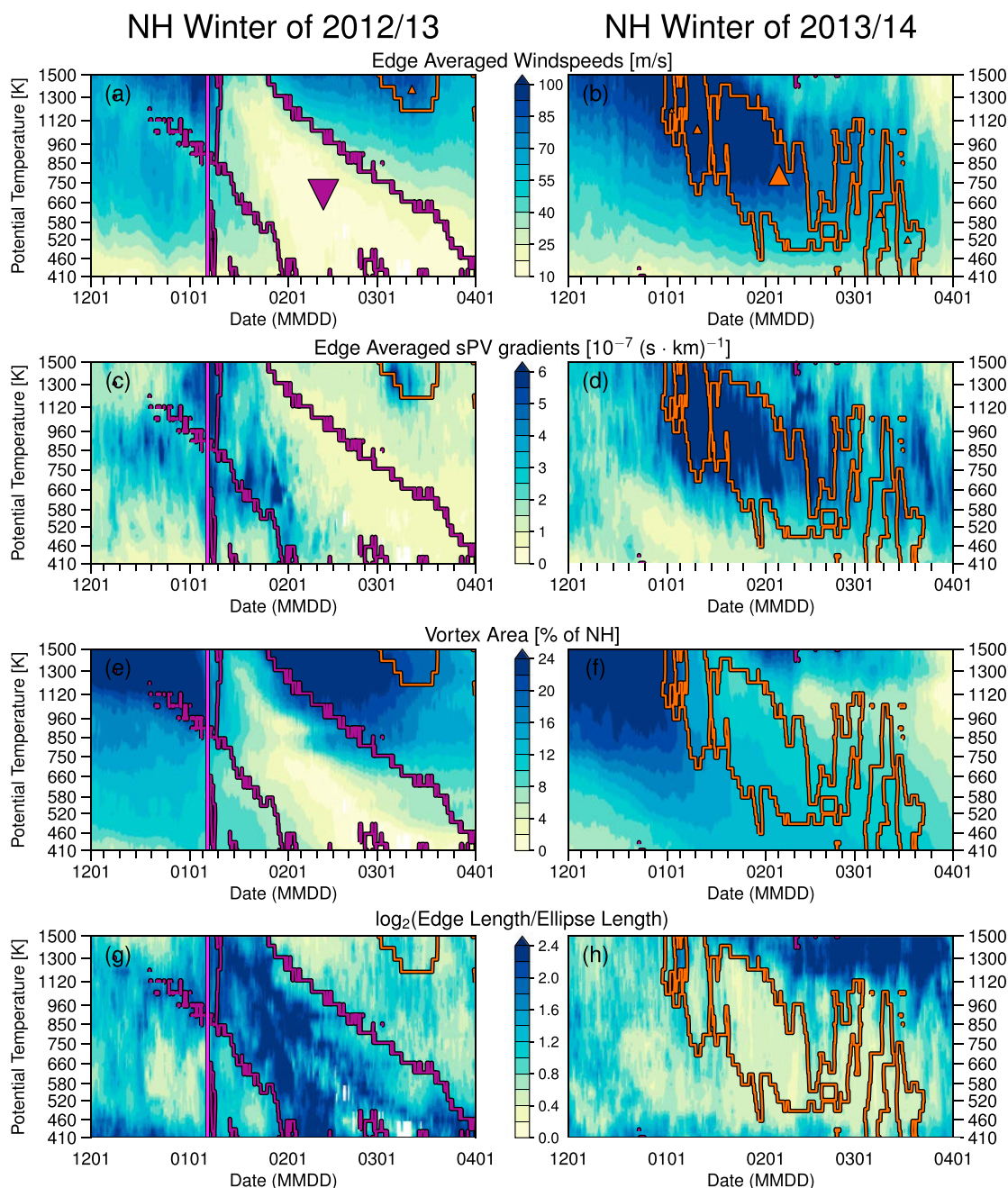
Figure 9. Example time series of some CAVE-ART diagnostics during a weak vortex event (NH winter 2012/2013 (Figures 9a, 9c, 9e, and 9g)) and a strong vortex event (NH winter 2013/2014 (Figures 9b, 9d, 9f, and 9h)). The diagnostics shown include wind speeds averaged around the (a, b) vortex edge, (c, d) horizontal-scaled PV gradients around the vortex edge, (e, f) vortex area, and (g, h) the log-length ratio of the vortex edge length to its equivalent ellipse circumference. Times and levels where the vortex is weak/strong are framed with purple/orange thick lines. In Figures 9a and 9b purple upside down triangles and orange upright triangles are plotted at the centroids of the event "objects" (see text) of the weak and strong events, respectively. The sizes of the triangles are proportional to the event area in time and potential temperature. The vertical magenta lines in Figures 9a, 9c, 9e, and 9g indicate the onset date of the January 2013 sudden warming event.

event of 2012/2013 (framed by purple lines), the vortex edge wind speeds rapidly decelerate as the vortex breaks down in shape and size. The vortex breaks down almost completely throughout the stratosphere during this time, simultaneously with the log-length ratio becoming very large, indicating a highly disturbed, even ill-defined, vortex region. In contrast, during the strong vortex event of 2013/2014 (framed by orange lines), the vortex edge wind speeds become very large (above 100 m s^{-1} at 850 K), concurrent with intense PV gradients in the vortex edge region. The vortex shrinks in the middle to upper stratosphere, but the log-length
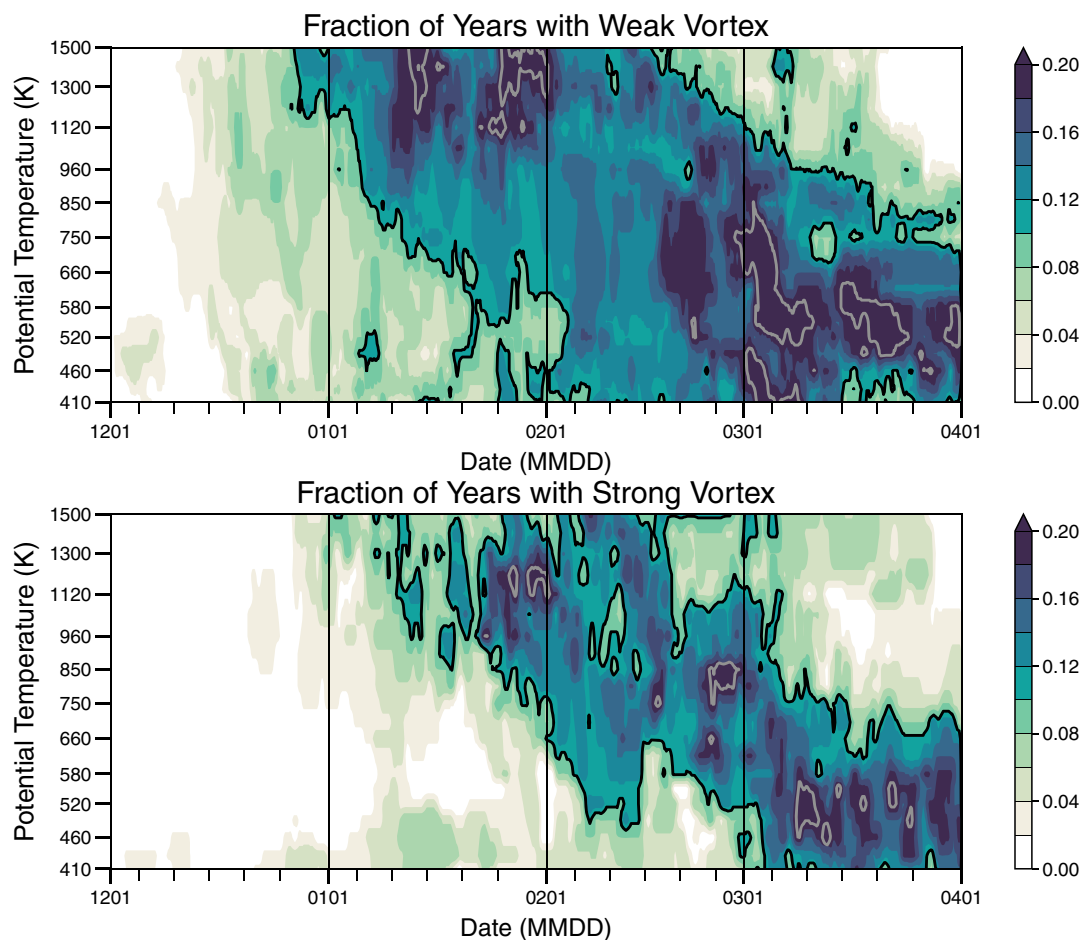
Figure 10. Frequencies of (top) weak and (bottom) strong vortex states as a function of potential temperature and time. The black and gray contour lines in both panels highlight where 10% and 20% of the years have a defined event at that specific time/level. Note that times and levels when and where the vortex is undefined by CAVE-ART are included in the weak vortex composite.

ratio remains small, indicating that the vortex was highly coherent and nearly elliptical during this time. The "jagged" appearance of the 2013/2014 strong vortex event(s) compared to the largely "monolithic" appearance of the 2012/2013 weak event is generally indicative of the comparatively short timescales of vortex intensification in different regions of the stratosphere where the vortex can intensify or subside rapidly over the course of periods as short as 3 to 5 days. This contrasts with the rapid onset of large weak events (which tend to be SSWs) that often have prolonged recoveries. These events also showcase other interesting features: For example, the large weak vortex event of 2012/2013 is succeeded by a small strong vortex event in the upper stratosphere, which is indicative of a rapid reformation of the middle and upper stratospheric vortex. In 2013/2014, the increase in vortex strength moves downward as the evolution of the vortex in the middle to upper stratosphere becomes complex, with growing and shrinking vortex area (in late January through February) concurrent with increasing values of log-length ratio and a deceleration of vortex edge wind speeds that coincide with the vortex becoming disturbed around the time of a split-like event (see Figure 5p).

Figure 10 shows the frequency of weak and strong vortex states at individual levels and times expressed as a fraction of the 38 NH winters of MERRA-2 data used in our analysis. The patterns of weak and strong events look morphologically similar, with frequencies above 0.1 (or one event/decade) beginning in the middle to upper stratosphere in January, filling most of the stratosphere through February, and localized maxima with frequencies exceeding 0.2 (or two events/decade) in the lower stratosphere in March. Overall, weak vortex events tend to be more frequent and fill more of the levels and times than strong vortex events; this is partly related to the fact that we include times and levels when the vortex is undefined (i.e., completely broken down)
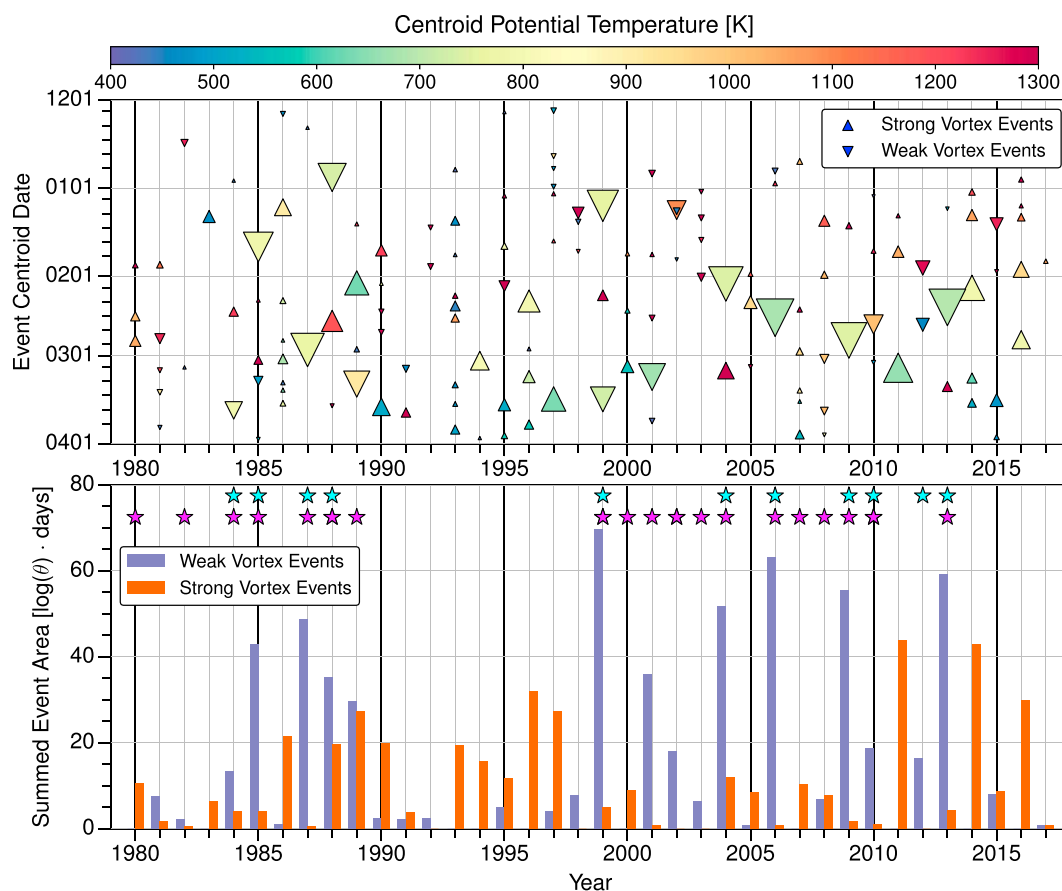
Figure 11. (top) Scatterplot time series of weak and strong vortex events and (bottom) barplot of winter-integrated weak and strong vortex events. In Figure 11 (top), the upside down/regular triangle symbols represent weak/strong vortex events; these symbols are plotted at the center of the event in time as determined by the event centroid (see main text) and are colored according to the events' centroid potential temperatures. Furthermore, the symbol sizes are proportional to the event area in log(θ)-time space. Note that time runs downward from 1 December to 1 April on the y axis. Figure 11 (bottom) shows the winter-integrated areas of events, with the purple/orange bars representing the total from weak/strong events during the DJFM season. The magenta/cyan stars highlight winters with major sudden warmings in MERRA-2/polar night jet oscillations.

as part of a weak vortex event but is primarily due to the fact that large weakening events (usually major SSWs) often propagate downward coherently from the upper stratosphere into the LMS (see Figures 9a, 9c, 9e, and 9g), whereas strong vortex events often rapidly subside and/or grow spontaneously (Figures 9b, 9d, 9f, and 9h) within specific regions of the stratosphere. The patterns are also affected by the seasonal cycle: for example, as seen in Figure 7, vortex edge wind speeds maximize in the upper stratosphere (above ~1000 K) between mid-December and late January, meaning that weak vortex events are more likely than strong events at these levels and times (as seen in Figure 10, top). Similarly, since wind speeds in the lower stratosphere do not increase much over DJF, strong events are more likely in the lowest levels at the end of the season when and if the vortex is long lived.

As seen in Figure 9, weak and strong vortex events defined using vortex edge wind speeds can span and vary across multiple vertical levels over time. Thus, to synthesize and condense this information to examine all 38 NH winters, we perform a simple moments analysis: At every time and level when and where the vortex is strong or weak, we flag the points to create binary masks that highlight weak/strong events. Single events are then any closed "blobs" in these binary masks (limited by boundaries at 410 and 1500 K and 1 December and 1 April); using time as the x coordinate, and log(θ) as the y coordinate, we then calculate geometric areas and centroids of these time/height cross sections of events. From this perspective, the event areas are indicative of the total size of any given weak/strong vortex event in both time and potential temperature, while the centroids represent the approximate center of the event. For example, the triangles in Figures 9a and 9b
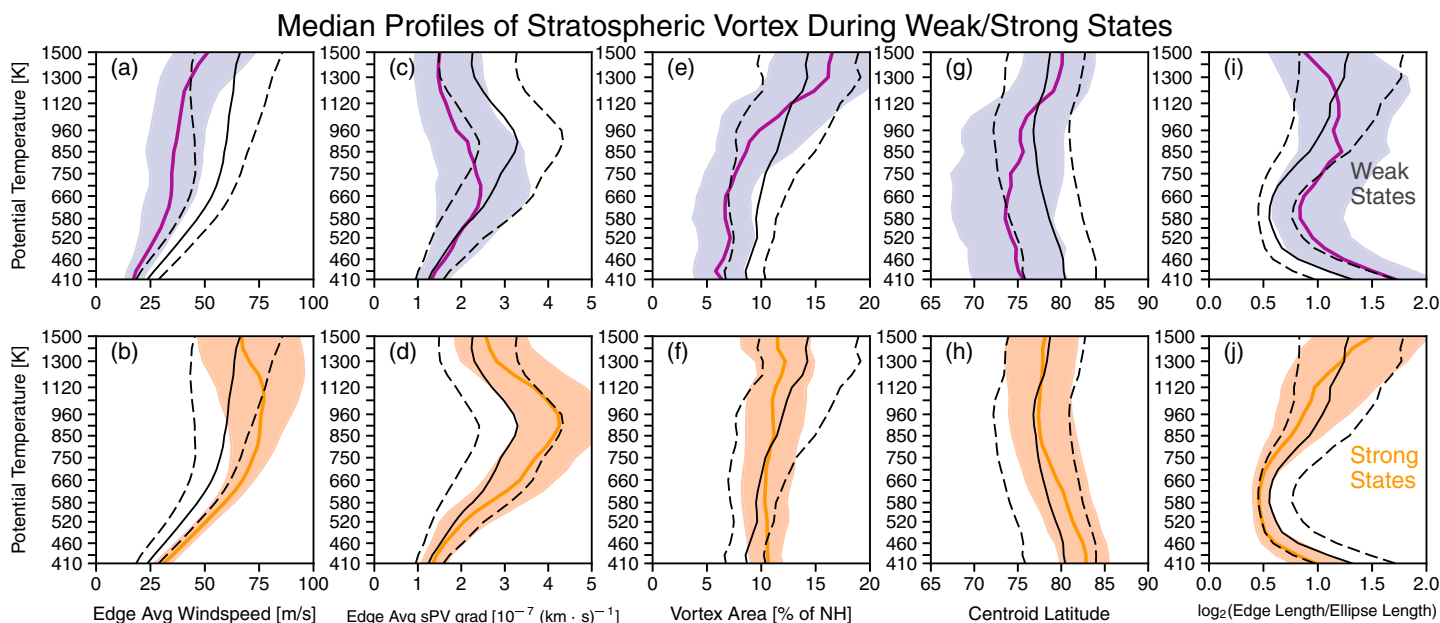
Figure 12. Profiles of CAVE-ART diagnostics composited by (a, c, e, g, i) weak and (b, d, f, h, j) strong vortex events. The thick colored lines indicate the median of the distributions, while the envelopes indicate the 25th–75th percentile range. The black solid/dashed lines indicate the full climatological median and 25th–75th percentile ranges from all MERRA-2 DJFM profiles. The diagnostics grouped in columns from left to right are vortex edge-averaged wind speeds, vortex edge-averaged sPV gradients, vortex area, centroid latitude, and the log-length ratio of the vortex edge to the equivalent ellipse circumference.

are plotted at the centroids of the event objects framed in purple and orange. In Figure 11 (top) we show a scatter plot with time on the *y* axis (going downward from 1 December to 1 April) and years on the *x* axis, with symbols of weak and strong vortex events plotted at their centroid date; the symbols are also colored according to their centroid potential temperature, and their size is proportional to the event area in the time-log(*θ*) space. Figure 11 (bottom) shows a bar plot with the total weak and strong event areas integrated over each winter. In these cases, we have filtered out small events consisting of less than 64 points in the binary masks mentioned above; this was done so that an event at a single isentropic level would have to last at least 8 days to be counted. Since these events are extremely unlikely to occur at only one level, the time stringency is relaxed to, for example, 2 days for an event spanning four isentropic surfaces. We have confirmed that this filtering does not qualitatively alter the results shown.

Figure 11 shows that weak vortex events defined using vortex edge wind speeds tend to be much larger than strong events. These weak events tend to have centroid potential temperatures around 700 to 800 K; these features arise primarily because these weak events are major SSWs that propagate downward from the upper stratosphere and disturb the full depth of the vortex over a continuous span of days to weeks, which gives rise to large event areas and centroid potential temperatures around the middle of the CAVE-ART vertical range. Strong vortex events, in contrast, tend to be more transient and localized, as discussed previously and shown in Figure 9. Years with relatively large winter-integrated strong event areas tend to have several small strong vortex events that occur over the duration of the season, indicating that in these cases the vortex is generally strong for long periods of time but not anomalously strong enough to be counted by our definition for long periods of time or over a wide range of levels. Many of the largest weak vortex years are years with polar night jet oscillation (PJO) events (e.g., Hitchcock et al., 2013, and references therein), which are the extended recovery periods following some SSWs that are marked by a rapid recovery of the vortex in the upper stratosphere and mesosphere. Sometimes this resurgence of the upper stratospheric vortex shows up as a strong vortex event at the high isentropic levels (e.g., see strong event following the 2013 SSW in Figure 9); years such as 1988, 1999, 2004, and 2013 show large weak vortex events that are followed by small strong vortex events at levels above 1000 K. However, not all PJO events show up as large weak vortex years; for example, 1984 and 2010 are both years in which PJOs occurred, but these weak events did not disturb the full vortex throughout the stratosphere. Along these same lines, years with major SSWs do not always have significant weak vortex events. In some cases this is tied to the seasonal cycle; some major SSWs occur in late February and March (e.g., 29 February 1980, 24 February 1984, and 20 March 2000) when the climatological vortex edge wind
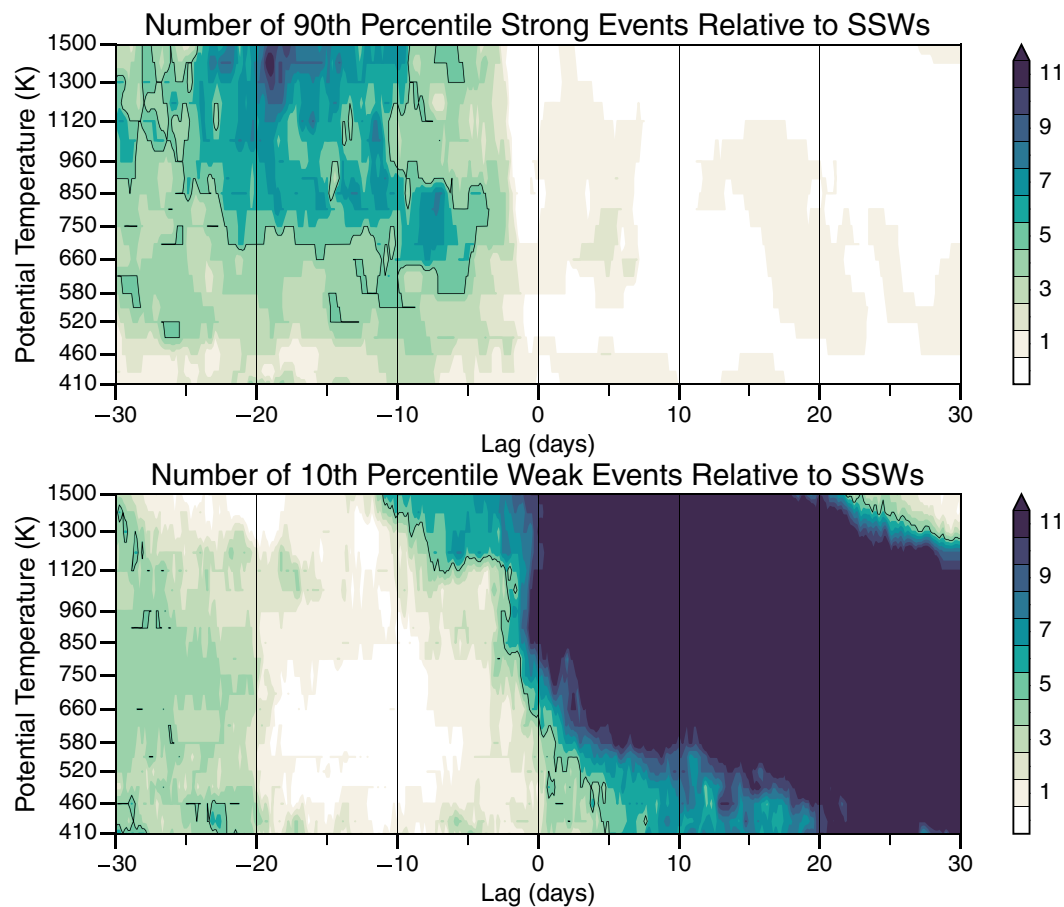
Figure 13. Number of (top) 90th percentile strong vortex events and (bottom) 10th percentile weak vortex events composited relative to the onset dates of MERRA-2 major sudden warmings. The black line contour indicates where the number of events aligned is greater than 5. Please see main text for strong/weak vortex definitions.

speeds are weak anyway, and thus, these major SSWs were not highly anomalous disturbances. In other cases, such as the early winter SSWs from 4 December 1981 and 18 January 2003, the disturbances to the vortex were very transient—these events strongly disturbed and distorted the vortex in the middle to upper stratosphere but had comparatively small effects in the lower stratosphere where the vortex stayed relatively elliptical and strong (not shown).

Figure 12 shows median profiles (along with 25th and 75th percentile envelopes) of some CAVE-ART diagnostics for composites of weak and strong events. Because the weak and strong vortex events typically do not span the full vortex at any given time, we include the full diagnostic profiles in the composites from any cases during DJFM when the vortex is detected as strong or weak at any level below 1200 K. Weak vortex states (Figures 12a, 12c, 12e, 12g, and 12i) show a particularly large range of variability, as seen in the wide first/third quartile envelopes. Especially during some large SSW events that propagate downward, the vortex can be disturbed in the upper stratosphere but not fully affected in the lower stratosphere until some time later. Nevertheless, the weak states do show features expected of a weak and less coherent vortex, including weaker winds and wind shear (Figure 12a), lower horizontal PV gradients in the edge region (Figure 12c), a smaller area in the lower stratosphere that increases with height (Figure 12e), a more equatorward displaced vortex core (Figure 12g), and a more distorted vortex edge (Figure 12i). In contrast, during strong states the vortex tends to have strong winds and enhanced wind shear (Figure 12b), larger PV gradients in the edge region (Figure 12d), a more pole centered and cylindrical shape (Figures 12f and 12h), and a less filamented edge (Figure 12j). These results indicate that examining characteristics of the vortex throughout the stratosphere can be useful for determining the overall strength of the vortex, regardless of the statistical extremity of any given diagnostic.

We do see some evidence in our results to suggest that strong and weak events are not necessarily independent. In particular, we found that when we relaxed our definition of weak and strong vortex events to use 10th/90th and 15th/85th percentiles for onset and termination, many weak vortex events (including but not limited to major SSWs) were preceded closely by strong vortex events in the middle to upper stratosphere. We do not show any of these specific events herein, but some such events, for example, in 1984 and 1989, can be seen in Figure 11. In Figure 13, we plot the number of these 10th/90th percentile weak/strong vortex events relative to the 25 onset dates of MERRA-2 major SSWs between 1979/1980 and 2016/2017, including the anomalously early final warmings from 12 March 2005 to 6 March 2016 (the results are not sensitive to these final warmings being excluded). As expected, there is a very high number of aligned weak events following these major SSW onset dates that saturate the colorbar (the local maximum of weak events 30–20 days prior to lag 0 is due to years with two SSWs). However, there is also a notable maximum in the number of strong events that align at time lags of around 25–10 days prior to the SSW onsets in the middle to upper stratosphere. These results may be evidence of something like vortex preconditioning (e.g., McIntyre, 1982). More work is necessary to determine whether there is a causal relationship, but some recent studies have listed conditions that could indicate such preconditioning, including decreased vortex area, enhanced PV gradients in the vortex edge region, and a more pole-centered vortex (see, e.g., Albers and Birner, 2014; Liu and Scott, 2015; Scott, 2016). These conditions are all characteristics of the vortex that are shared with the strong vortex composites shown in Figure 12. In describing the onset stage (37 to 23 days prior) to sudden warming events, Limpasuvan et al. (2004) noted that the zonal flow is anomalously strong and the vortex anomalously pole centered. Birner and Albers (2017) also noted that the vortex was anomalously strong prior to those sudden stratospheric deceleration events (see their definitions) that were preceded by lower tropospheric wave events (see, e.g., their supporting information Figure S1). The results shown in Figure 13 seem to at least confirm that from the vortex-centered view of CAVE-ART, the vortex is anomalously strong prior to many sudden warming events. We also emphasize that this result generalizes to other non-SSW weak events as well.

5. Conclusions and Discussion

We have used computer vision techniques to comprehensively characterize the Arctic stratospheric polar vortex in MERRA-2 reanalysis data. Part of our motivation for this paper was to advocate for the use of computer vision and image processing techniques and show their applicability as analysis tools for data sets that are not necessarily digital images. Computer vision and image processing are mature fields with large bodies of literature available. In addition, many of the most useful techniques are widely (often freely) available in software libraries, including the most common scientific programming languages. While the material presented herein focused on using computer vision techniques applied to characterize polar vortices as material entities, we also applied the same computer vision techniques discussed in section 2 to segment and describe features in potential temperature/time series data in section 4.2; a similar method was used by Albers et al. (2016) to analyze features in longitude-time series data sets. These examples demonstrate the broad applicability of computer vision and image processing techniques to multidimensional data sets.

We have applied segmentation, descriptive, and tracking algorithms to the stratospheric polar vortex. Polar vortices generally represent a well-posed problem for such computer vision techniques because they are long lived, materially large, and easily defined throughout the stratosphere. They can also split, become displaced, and/or filament during vortex disturbances, which are events that can be easily diagnosed with segmentation of vortex regions, region descriptors, and/or diagnostics of the vortex edge. To this end, we developed the Characterization and Analysis of Vortex Evolution using Algorithms for Region Tracking (CAVE-ART) package, which utilizes the aforementioned techniques to describe and catalog the state of the stratospheric polar vortex throughout a winter season. As described in section 3.2, CAVE-ART uses potential vorticity (PV) data to define the vortex: It segments all regions of high PV larger than a given vortex edge value, filters out regions too small to be a valid vortex, calculates object descriptors of the valid vortex regions, and tracks the individual vortex regions through time. CAVE-ART can thus calculate a large suite of diagnostics, including those that characterize the vortex edge, for every individual vortex region.

Using the results from CAVE-ART, we defined and cataloged an expanded set of split-like vortex events. Our detection algorithm found 52 potential events between 1979/1980 and 2016/2017, of which we subjectively classified 38 as split like, 10 as dubious, and 4 as false positives. While our classification scheme includes a final subjective step, it nevertheless highlights the value of the computer vision techniques used in CAVE-ART

to identify events of interest for further study without having to pore through daily PV maps on multiple vertical levels. Since CAVE-ART and our detection algorithm are based on computer vision techniques, we thought it appropriate to visually inspect all of the events detected and make them available. Our catalog of events, albeit large, should not be considered comprehensive, foremost because we only include events from DJFM even though split events can occur in October and November. Also, while we expect that it is rare, it is possible for CAVE-ART to miss events because we use constant PV values for the vortex edge that may not split during some events; we mitigated this possibility by looking for splitting across multiple isentropic levels and requiring that a split have only a relatively short duration.

The relatively large number of split-like disturbances identified herein provides evidence that events of interest could be going ignored because of common reliance on specific dynamical definitions (such as major SSW criteria) being met, time-based thresholds (such as requiring events to be separated by 20–30 days), and/or the use of single levels to characterize vortex evolution. However, the diversity among the split-like events shown in Figures 4 and 5 beg some questions, including the following: How do events that arise primarily in the lower stratosphere differ from those that clearly penetrate throughout the stratosphere? Is there a minimum size and/or vertical depth that a vortex offspring must have to be considered part of a valid split event? It would be interesting to compare the different events presented herein, particularly in light of recent studies that suggest alternative mechanisms for vortex splitting events (e.g., Liu and Scott, 2015; Matthewman and Esler, 2011; O'Neill et al., 2017; Scott, 2016, and references therein) and studies that point out issues with models' capabilities to forecast such vortex splits (e.g., Taguchi, 2016; Tripathi et al., 2016). Assessing these processes/issues for events, including those that are transient or limited in vertical extent, could provide valuable insight into splitting mechanisms and their representation in models.

As seen in previous studies, moment-based methods can be helpful for identifying vortex splits (e.g., Matthewman et al., 2009; Matthewman & Esler, 2011; Mitchell et al., 2013; Seviour et al., 2013). We thus compared our segmentation-based detection of split-like events with methods that use thresholds of the aspect ratio (Seviour et al., 2013) and excess kurtosis (Matthewman & Esler, 2011, 2009). In many cases the moments and segmentation-based approaches agree well. However, it is possible for the aspect ratio and excess kurtosis methods to identify as splits events where the vortex only becomes very elongated and/or pinched; these diagnostics may also miss potential events due to highly unequal sizes of the offspring vortices, and the excess kurtosis in particular is highly sensitive to filamentation. All detection methods rely on defining a vortex edge contour, and, as discussed above, this can affect any method. An approach combining both the moments and segmentation-based strategies has the potential to address the weaknesses of each individual approach without having to analyze multiple contours. CAVE-ART catalogs enough information to develop such a hybrid approach, but it is beyond the scope of this study.

As a further application of CAVE-ART and computer vision techniques, we introduced a diagnostic of vortex strength based on extreme values of vortex edge wind speed anomalies. This diagnostic is complementary to commonly used measures of vortex strength such as annular mode indices (e.g., Dunn-Sigouin & Shaw, 2015, and references therein) or those based on zonal mean zonal winds (e.g., Tripathi, Charlton-Perez, et al., 2015, and references therein), as it is independent of the location and size of the vortex. For example, whereas zonal mean zonal winds in the stratosphere can decrease simply by the vortex becoming displaced (which certainly constitutes a vortex disturbance), vortex edge wind speeds could theoretically show little disturbance if the vortex remained coherent and strong. Our analysis also combines vortex strength information across multiple levels. By identifying weak and strong events as closed regions in potential temperature and time (see Figure 9), we defined the centers of these extreme events in time and potential temperature and compared their relative sizes. Our results highlight the wide spectrum of behavior exhibited by the Arctic polar vortex in both time and altitude, which includes small localized weak/strong events, as well as prolonged and vertically deep ones. Distinguishing between such "major" and "minor" events has recently been highlighted by many as important for more completely describing the full variability of the stratosphere and its importance for numerous research topics including definitions of sudden warming events (e.g., Butler et al., 2015; Maury et al., 2016), polar chemical processing and ozone loss (e.g., Manney & Lawrence, 2016; Strahan et al., 2016), coupling with the troposphere (e.g., Dunn-Sigouin & Shaw, 2015; Runde et al., 2016), understanding climate connections to, for example, the quasi-biennial oscillation and El Niño/La Niña (e.g., Díaz-Durán et al., 2017; Garfinkel et al., 2010; Iza et al., 2016), forecasting and prediction (e.g., Butler et al., 2016; Tripathi, Charlton-Perez, et al., 2015), and defining and attributing events in climate models (e.g., Ayarzagüena et al., 2015; Kim et al., 2017).

Not all major SSWs appear as weak vortex events with our definition based on vortex edge wind speed anomalies. In some cases these SSWs are "invisible" (or nearly so) because they occur late in the season; in others, the disturbances are simply too transient or limited in altitude to strongly disturb the vortex as a whole. Thus, even major SSWs show large variability in the degree to which they affect the vortex. CAVE-ART provides enough diagnostics to quantify and characterize such vortex disturbances; furthermore, the capability to detect minor warming-like disturbances with our weak vortex events can allow for comparisons of these events. Such work could help determine the conditions under which event definitions based on zonal mean views and/or on a single level are inadequate for identifying and characterizing stratospheric disturbances. In addition, we have shown some qualitative evidence that strong and weak states of the vortex may in some cases be linked in a manner resembling vortex preconditioning. Our vortex strength definition, combined with other CAVE-ART diagnostics, could be useful for identifying preconditioned states of the vortex prior to weak vortex events, including major and minor sudden warming disturbances. Perhaps more importantly, diagnostics from CAVE-ART could assist in further understanding the physics through which the stratospheric vortex strengthens and weakens in such extreme ways by helping to reconcile views based on wave mean flow interactions of upward propagating waves (e.g., Limpasuvan et al., 2004, 2005; Matsuno, 1971; Nishii et al., 2009), nonlocal wave effects (e.g., Esler & Matthewman, 2011; Harnik, 2009; Matthewman & Esler, 2011; Plumb, 1981; Shaw & Perlwitz, 2013), and internal stratospheric control (e.g., Birner & Albers, 2017; de la Cámara et al., 2017; Hitchcock & Haynes, 2016; Scott & Polvani, 2004, 2006) with the dynamics in the frame of reference of the vortex itself.

The results presented here show examples of how the CAVE-ART package can be valuable for studies focused on stratospheric vortices and, more generally, how powerful computer vision techniques are as tools for numerous geophysical applications. Some work in progress using CAVE-ART includes an investigation of vortex preconditioning, characterizations of Antarctic vortex evolution, and an evaluation of relationships between the Northern Annular Mode, zonal mean zonal winds, and the vortex characteristics cataloged by CAVE-ART.

Appendix A: Split-Like Event Detection Sensitivity

In section 4.1, we described the criteria we used to detect *potential* split-like vortex events. For the events shown in the main text, we considered a potential event to be detected if, between the 14 isentropic levels from 430 to 960 K, at least 4 consecutive isentropic levels had flagged onset dates pooled together and/or if at least 7 of the 14 isentropic levels were in a grouping of onset dates. With these parameters (and others whose choices and sensitivities were discussed in the main text), we found 52 potential events that we visually inspected and subdivided into 38 valid split-like events, 10 dubious events, and 4 false positives. When we required only three consecutive isentropic levels, we obtained 94 potential events; while this includes the 52 events originally found, we did not visually inspect all of the additional 42 potential events. Of those that we did inspect, we only found what we would consider false positives. When we required 5 consecutive isentropic levels, we obtained 33 potential events, of which we would consider 27 to be split-like, 5 to be dubious, and 1 to be a false positive; the 11 split-like events that drop out in this case (from going from 38 to 27 valid events) are those that clearly have less vertical coherence (e.g., those in February 1995 and February 2004) and also those where the vortex edge contours we use are slightly too low for the vortex to be seen as split at five consecutive levels (e.g., those in January 2003 and February 2007). We also found that the additional possible detection requirement, that 7 of the 14 isentropic levels be in a grouping, was never necessary for the detection of split-like events because the first consecutive level requirement was always met. However, we included this condition to account for the possibility that issues with our vortex edge contours being too low in some cases could show a split at the majority of levels but in disconnected groupings of consecutive levels.

References

Albers, J. R., & Birner, T. (2014). Vortex preconditioning due to planetary and gravity waves prior to sudden stratospheric warmings. *Journal of Atmospheric Sciences*, 71, 4028–4054.

Albers, J. R., Kiladis, G. N., Birner, T., & Dias, J. (2016). Tropical upper-tropospheric potential vorticity intrusions during sudden stratospheric warmings. *Journal of Atmospheric Sciences*, 73(6), 2361–2384. https://doi.org/10.1175/JAS-D-15-0238.1

Allen, D. R., & Nakamura, N. (2001). A seasonal climatology of effective diffusivity in the stratosphere. *Journal of Geophysical Research*, 106, 7917–7935.

Andrews, D. G. (1989). Some comparisons between the middle atmosphere dynamics for the Southern and Northern Hemispheres. *Pure and Applied Geophysics*, 130, 213–232.

Arnaud, Y., Desbois, M., & Maizi, J. (1992). Automatic tracking and characterization of African convective systems on Meteosat pictures. *Journal of Applied Meteorology*, *31*(5), 443–453. https://doi.org/10.1175/1520-0450(1992)031<0443:ATACOA>2.0.CO;2

Ayarzagüena, B., Orsolini, Y. J., Langematz, U., Abalichin, J., & Kubin, A. (2015). The relevance of the location of blocking highs for stratospheric variability in a changing climate. *Journal of Climate*, *28*(2), 531–549. https://doi.org/10.1175/JCLI-D-14-00210.1

Baldwin, M. P., & Dunkerton, T. J. (2001). Stratospheric harbingers of anomalous weather regimes. *Science*, *294*, 581–584.

Baldwin, M. P., & Holton, J. R. (1988). Climatology of the stratospheric polar vortex and planetary wave breaking. *Journal of Atmospheric Sciences*, *45*, 1123–1142.

Birner, T., & Albers, J. R. (2017). Sudden stratospheric warmings and anomalous upward wave activity flux. *Scientific Online Letters on the Atmosphere*, *13A*(Special Edition), 8–12. https://doi.org/10.2151/sola.13A-002

Bloom, S. C., Takacs, L. L., da Silva, A. M., & Ledvina, D. (1996). Data assimilation using incremental analysis updates. *Monthly Weather Review*, *124*, 1256–1271.

Butchart, N., & Remsberg, E. E. (1986). The area of the stratospheric polar vortex as a diagnostic for tracer transport on an isentropic surface. *Journal of Atmospheric Sciences*, *43*, 1319–1339.

Butler, A. H., Arribas, A., Athanassiadou, M., Baehr, J., Calvo, N., Charlton-Perez, A., ... Yasuda, T. (2016). The Climate-system Historical Forecast Project do stratosphere-resolving models make better seasonal climate predictions in boreal winter? *Quarterly Journal of the Royal Meteorological Society*, *142*(696), 1413–1427. https://doi.org/10.1002/qj.2743

Butler, A. H., Seidel, D. J., Hardiman, S. C., Butchart, N., Birner, T., & Match, A. (2015). Defining sudden stratospheric warmings. *Bulletin of the American Meteorological Society*, *96*(11), 1913–1928. https://doi.org/10.1175/BAMS-D-13-00173.1

Butler, A. H., Sjoberg, J. P., Seidel, D. J., & Rosenlof, K. H. (2017). A sudden stratospheric warming compendium. *Earth System Science Data*, *9*(1), 63–76. https://doi.org/10.5194/essd-9-63-2017

Charlton, A. J., & Polvani, L. M. (2007). A new look at stratospheric sudden warmings. Part I: Climatology and modeling benchmarks. *Journal of Climate*, *20*, 449–469.

Dameris, M., Wirth, M., Renger, W., & Grewe, V. (1995). Definition of the polar vortex edge by LIDAR data of the stratospheric aerosol: A comparison with values of potential vorticity (Tech. Rep 26). Institut für Physik der Atmosphäre, DLR.

de la Cámara, A., Albers, J. R., Birner, T., Garcia, R. R., Hitchcock, P., Kinnison, D. E., & Smith, A. K. (2017). Sensitivity of sudden stratospheric warmings to previous stratospheric conditions. *Journal of Atmospheric Sciences*, *74*(9), 2857–2877. https://doi.org/10.1175/JAS-D-17-0136.1

Dias, J., Tulich, S. N., & Kiladis, G. N. (2012). An object-based approach to assessing the organization of tropical convection. *Journal of Atmospheric Sciences*, *69*(8), 2488–2504. https://doi.org/10.1175/JAS-D-11-0293.1

Díaz-Durán, A., Serrano, E., Ayarzagüena, B., Abalos, M., & de la Cámara, A. (2017). Intra-seasonal variability of extreme boreal stratospheric polar vortex events and their precursors. *Climate Dynamics*, 1–19. https://doi.org/10.1007/s00382-017-3524-1

Dunkerton, T. J., & Delisi, D. P. (1986). Evolution of potential vorticity in the winter stratosphere of January-February 1979. *Journal of Geophysical Research*, *91*, 1199–1208.

Dunn-Sigouin, E., & Shaw, T. A. (2015). Comparing and contrasting extreme stratospheric events, including their coupling to the tropospheric circulation. *Journal of Geophysical Research*, *120*, 1374–1390. https://doi.org/10.1002/2014JD022116

Esler, J. G., & Matthewman, N. J. (2011). Stratospheric sudden warmings as self-tuning resonances. Part II: Vortex displacement events. *Journal of Atmospheric Sciences*, *68*(11), 2505–2523. https://doi.org/10.1175/JAS-D-11-08.1

Freeman, H. (1970). *Boundary encoding and processing. Picture processing and psychopictorics* (pp. 241–263). New York: Academic Press.

Garfinkel, C. I., Hartmann, D. L., & Sassi, F. (2010). Tropospheric precursors of anomalous Northern Hemisphere stratospheric polar vortices. *Journal of Climate*, *23*(12), 3282–3299. https://doi.org/10.1175/2010JCLI3010.1

Gelaro, R., McCarty, W., Suárez, M. J., Todling, R., Molod, A., Takacs, L., ... Zhao, B. (2017). The Modern-Era Retrospective analysis for Research and Applications, Version 2 (MERRA-2). *Journal of Climate*, *30*(14), 5419–5454. https://doi.org/10.1175/JCLI-D-16-0758.1

Geraets, W., van Daatselaar, A., & Verheij, J. (2004). An efficient filling algorithm for counting regions. *Computer Methods and Programs in Biomedicine*, *76*(1), 1–11. https://doi.org/10.1016/j.cmpb.2003.09.004

Global Modeling and Assimilation Office (2015). MERRA-2 inst3_3d_asm_Nv: 3d,3-Hourly, Instantaneous, Model-Level, Assimilation, Assimilated Meteorological Fields V5.12.4. https://doi.org/10.5067/WWQSXQ8IVFW8 (Accessed 06-07-2017).

Hannachi, A., Mitchell, D., Gray, L., & Charlton-Perez, A. (2011). On the use of geometric moments to examine the continuum of sudden stratospheric warmings. *Journal of Atmospheric Sciences*, *68*(3), 657–674. https://doi.org/10.1175/2010JAS3585.1

Haralick, R. M., & Shapiro, L. G. (1985). Image segmentation techniques. *Computer Vision, Graphics, and Image Processing*, *29*(1), 100–132. https://doi.org/10.1016/S0734-189X(85)90153-7

Harnik, N. (2009). Observed stratospheric downward reflection and its relation to upward pulses of wave activity. *Journal of Geophysical Research*, *114*, D08120. https://doi.org/10.1029/2008JD010493

Harvey, V. L., Randall, C. E., & Hitchman, M. H. (2009). Breakdown of potential vorticity-based equivalent latitude as a vortex-centered coordinate in the polar winter mesosphere. *Journal of Geophysical Research*, *114*, D22105. https://doi.org/10.1029/2009JD012681

Haynes, P., & Shuckburgh, E. (2000). Effective diffusivity as a diagnostic of atmospheric transport 1. Stratosphere. *Journal of Geophysical Research*, *105*, 22,777–22,794.

Hitchcock, P., & Haynes, P. H. (2016). Stratospheric control of planetary waves. *Geophysical Research Letters*, *43*, 11,884–11,892. https://doi.org/10.1002/2016GL071372

Hitchcock, P., Shepherd, T. G., & Manney, G. L. (2013). Statistical characterization of Arctic polar-night jet oscillation events. *Journal of Climate*, *26*, 2096–2116.

Hodges, K. I. (1994). A general method for tracking analysis and its application to meteorological data. *Monthly Weather Review*, *122*(11), 2573–2586. https://doi.org/10.1175/1520-0493(1994)122<2573:AGMFTA>2.0.CO;2

Hodges, K. I. (1995). Feature tracking on the unit-sphere. *Monthly Weather Review*, *123*, 3458–3465.

Hodges, K. I. (1999). Adaptive constraints for feature tracking. *Monthly Weather Review*, *127*(6), 1362–1373.

Horowitz, S. L., & Pavlidis, T. (1976). Picture segmentation by a tree traversal algorithm. *Journal of the ACM*, *23*(2), 368–388. https://doi.org/10.1145/321941.321956

Hoskins, B. J., McIntyre, M. E., & Robertson, A. W. (1985). On the use and significance of isentropic potential-vorticity maps. *Quarterly Journal of the Royal Meteorological Society*, *111*, 877–946.

Hu, J., Ren, R., & Xu, H. (2014). Occurrence of winter stratospheric sudden warming events and the seasonal timing of spring stratospheric final warming. *Journal of Atmospheric Sciences*, *71*(7), 2319–2334. https://doi.org/10.1175/JAS-D-13-0349.1

Hu, M.-K. (1962). Visual pattern recognition by moment invariants. *Information Theory, IRE Transactions on*, *8*(2), 179–187.

Iza, M., Calvo, N., & Manzini, E. (2016). The stratospheric pathway of La Niña. *Journal of Climate*, *29*(24), 8899–8914. https://doi.org/10.1175/JCLI-D-16-0230.1

Jung, T., & Barkmeijer, J. (2006). Sensitivity of the tropospheric circulation to changes in the strength of the stratospheric polar vortex. *Monthly Weather Review*, *134*(8), 2191–2207. https://doi.org/10.1175/MWR3178.1

Kim, J., Son, S.-W., Gerber, E. P., & Park, H.-S. (2017). Defining sudden stratospheric warming in climate models: Accounting for biases in model climatologies. *Journal of Climate*, *30*(14), 5529–5546. https://doi.org/10.1175/JCLI-D-16-0465.1

Kuroda, Y. (2008). Effect of stratospheric sudden warming and vortex intensification on the tropospheric climate. *Journal of Geophysical Research*, *113*, D15110. https://doi.org/10.1029/2007JD009550

Lawrence, Z. D., Manney, G. L., Minschwaner, K., Santee, M. L., & Lambert, A. (2015). Comparisons of polar processing diagnostics from 34 years of the ERA-Interim and MERRA reanalyses. *Atmospheric Chemistry and Physics*, *15*(7), 3873–3892. https://doi.org/10.5194/acp-15-3873-2015

Limbach, S., Schömer, E., & Wernli, H. (2012). Detection, tracking and event localization of jet stream features in 4-D atmospheric data. *Geoscientific Model Development*, *5*, 457–470.

Limpasuvan, V., Hartmann, D. L., Thompson, D. W. J., Jeev, K., & Yung, Y. L. (2005). Stratosphere-troposphere evolution during polar vortex intensification. *Journal of Geophysical Research*, *110*, D24101. https://doi.org/10.1029/2005JD006302

Limpasuvan, V., Thompson, D. W. J., & Hartmann, D. L. (2004). The life cycle of the Northern Hemisphere sudden stratospheric warmings. *Journal of Climate*, *17*(13), 2584–2596. https://doi.org/10.1175/1520-0442(2004)017<2584:TLCOTN>2.0.CO;2

Liu, Y. S., & Scott, R. K. (2015). The onset of the barotropic sudden warming in a global model. *Quarterly Journal of the Royal Meteorological Society*, *141*(693), 2944–2955. https://doi.org/10.1002/qj.2580

Lorensen, W. E., & Cline, H. E. (1987). Marching cubes: A high resolution 3D surface construction algorithm. *SIGGRAPH Computer Graphics*, *21*(4), 163–169. https://doi.org/10.1145/37402.37422

Manney, G. L., & Lawrence, Z. D. (2016). The major stratospheric final warming in 2016: Dispersal of vortex air and termination of Arctic chemical ozone loss. *Atmospheric Chemistry and Physics*, *16*, 15,371–15,396. https://doi.org/10.5194/acp-16-15371-2016

Manney, G. L., Daffer, W. H., Zawodny, J. M., Bernath, P. F., Hoppel, K. W., Walker, K. A., . . . Waters, J. W. (2007). Solar occultation satellite data and derived meteorological products: Sampling issues and comparisons with Aura Microwave Limb Sounder. *Journal of Geophysical Research*, *112*, D24S50. https://doi.org/10.1029/2007JD008709

Manney, G. L., Lawrence, Z. D., Santee, M. L., Livesey, N. J., Lambert, A., & Pitts, M. C. (2015). Polar processing in a split vortex: Arctic ozone loss in early winter 2012/2013. *Atmospheric Chemistry and Physics*, *15*(10), 5381–5403. https://doi.org/10.5194/acp-15-5381-2015

Manney, G. L., Santee, M. L., Rex, M., Livesey, N. J., Pitts, M. C., Veefkind, P., . . . Zinoviev, N. S. (2011). Unprecedented Arctic ozone loss in 2011. *Nature*, *478*, 469–475.

Manney, G. L., Zurek, R. W., Gelman, M. E., Miller, A. J., & Nagatani, R. (1994). The anomalous Arctic lower stratospheric polar vortex of 1992–1993. *Geophysical Research Letters*, *21*, 2405–2408.

Matsuno, T. (1971). A dynamical model of the stratospheric sudden warming. *Journal of the Atmospheric Sciences*, *28*(8), 1479–1494. https://doi.org/10.1175/1520-0469(1971)028<1479:ADMOTS>2.0.CO; 2

Matthewman, N. J., & Esler, J. G. (2011). Stratospheric sudden warmings as self-tuning resonances. Part I: Vortex splitting events. *Journal of Atmospheric Sciences*, *68*(11), 2481–2504. https://doi.org/10.1175/JAS-D-11-07.1

Matthewman, N. J., Esler, J. G., Charlton-Perez, A. J., & Polvani, L. M. (2009). A new look at stratospheric sudden warmings. Part III: Polar vortex evolution and vertical structure. *Journal of Climate*, *22*, 1566–1585.

Maury, P., Claud, C., Manzini, E., Hauchecorne, A., & Keckhut, P. (2016). Characteristics of stratospheric warming events during Northern winter. *Journal of Geophysical Research*, *121*, 5368–5380. https://doi.org/10.1002/2015JD024226

Maycock, A. C., & Hitchcock, P. (2015). Do split and displacement sudden stratospheric warmings have different annular mode signatures? *Geophysical Research Letters*, *42*, 10,943–10,951. https://doi.org/10.1002/2015GL066754

McIntyre, M. E. (1982). How well do we understand the dynamics of stratospheric warmings? *Journal of the Meteorological Society of Japan. Ser. II*, *60*(1), 37–65. https://doi.org/10.2151/jmsj1965.60.1_37

McIntyre, M. E. (1995). The stratospheric polar vortex and sub-vortex: Fluid dynamics and midlatitude ozone loss. *Philosophical Transactions of the Royal Society of London A*, *352*, 227–240.

McIntyre, M. E., & Palmer, T. N. (1983). Breaking planetary waves in the stratosphere. *Nature*, *305*, 593–600.

McIntyre, M. E., & Palmer, T. N. (1984). The "surf zone" in the stratosphere. *Journal of Atmospheric and Solar-Terrestrial Physics*, *46*, 825–849.

Mehtre, B. M., Kankanhalli, M. S., & Lee, W. F. (1997). Shape measures for content based image retrieval: A comparison. *Information Processing & Management*, *33*(3), 319–337. https://doi.org/10.1016/S0306-4573(96) 00069-6

Mitchell, D. M., Charlton-Perez, A. J., & Gray, L. J. (2011). Characterizing the variability and extremes of the stratospheric polar vortices using 2D moment analysis. *Journal of Atmospheric Sciences*, *68*, 1194–1213.

Mitchell, D. M., Gray, L. J., Anstey, J., Baldwin, M. P., & Charlton-Perez, A. J. (2013). The influence of stratospheric vortex displacements and splits on surface climate. *Journal of Climate*, *26*, 2668–2682.

Muelder, C., & Ma, K.-L. (2009). Interactive feature extraction and tracking by utilizing region coherency. In *Visualization Symposium, 2009. PacificVis' 09. IEEE Pacific* (pp. 17–24). IEEE.

Nakamura, N. (1996). Two-dimensional mixing, edge formation, and permeability diagnosed in an area coordinate. *Journal of Atmospheric Sciences*, *53*(11), 1524–1537. https://doi.org/10.1175/1520-0469(1996)053<1524:TDMEFA>2.0.CO;2

Nakamura, N., & Ma, J. (1997). Modified Lagrangian-mean diagnostics of the stratospheric polar vortices 2. Nitrous oxide and seasonal barrier migration in the Cryogenic Limb Array Etalon Spectrometer and SKYHI general circulation model. *Journal of Geophysical Research*, *102*, 25,721–25,735.

Nash, E. R., Newman, P. A., Rosenfield, J. E., & Schoeberl, M. R. (1996). An objective determination of the polar vortex using Ertel's potential vorticity. *Journal of Geophysical Research*, *101*, 9471–9478.

Nishii, K., Nakamura, H., & Miyasaka, T. (2009). Modulations in the planetary wave field induced by upward-propagating rossby wave packets prior to stratospheric sudden warming events: A case-study. *Quarterly Journal of the Royal Meteorological Society*, *135*(638), 39–52. https://doi.org/10.1002/qj.359

Nixon, M. S., & Aguado, A. S. (2012). *Feature extraction & image processing for computer vision*. New York: Academic Press.

O'Neill, A., Oatley, C. L., Charlton-Perez, A. J., Mitchell, D. M., & Jung, T. (2017). Vortex splitting on a planetary scale in the stratosphere by cyclogenesis on a subplanetary scale in the troposphere. *Quarterly Journal of the Royal Meteorological Society*, *143*(703), 691–705. https://doi.org/10.1002/qj.2957

Pal, N. R., & Pal, S. K. (1993). A review on image segmentation techniques. *Pattern Recognition*, *26*(9), 1277–1294. https://doi.org/10.1016/0031-3203(93)90135-J

Paparella, F., Babiano, A., Basdevant, C., Provenzale, A., & Tanga, P. (1997). A lagrangian study of the Antarctic polar vortex. *Journal of Geophysical Research*, *102*(D6), 6765–6773. https://doi.org/10.1029/96JD03377

Pavlidis, T. (1982). *Algorithms for graphics and image processing*. Berlin: Springer Science & Business Media.

Plumb, R. A. (1981). Instability of the distorted polar night vortex: A theory of stratospheric warmings. *Journal of Atmospheric Sciences*, *38*(11), 2514–2531. https://doi.org/10.1175/1520-0469(1981)038<2514:IOTDPN>2.0.CO;2

Reinders, F., Post, F. H., & Spoelder, H. J. W. (1999). Attribute-based feature tracking. In E. Gröller, H. Löffelmann, & W. Ribarsky (Eds.), *Data Visualization* Eurographics (Vol. 99, pp. 63–72). Vienna: Springer.

Rummukainen, M., Knudsen, B., & von der Gathen, P. (1994). Dynamical diagnostics of the edges of the polar vortices. *Annales Geophysicae*, *12*, 1114–1118.

Runde, T., Dameris, M., Garny, H., & Kinnison, D. E. (2016). Classification of stratospheric extreme events according to their downward propagation to the troposphere. *Geophysical Research Letters*, *43*, 6665–6672. https://doi.org/10.1002/2016GL069569

Samet, H. (1981). Connected component labeling using quadtrees. *Journal of the ACM*, *28*(3), 487–501. https://doi.org/10.1145/322261.322267

Schoeberl, M. R., & Hartmann, D. L. (1991). The dynamics of the stratospheric polar vortex and its relation to springtime ozone depletions. *Science*, *251*, 46–52.

Schoeberl, M. R., Lait, L. R., Newman, P. A., & Rosenfield, J. E. (1992). The structure of the polar vortex. *Journal of Geophysical Research*, *97*, 7859–7882.

Scott, R. K. (2016). A new class of vacillations of the stratospheric polar vortex. *Quarterly Journal of the Royal Meteorological Society*, *142*(698), 1948–1957. https://doi.org/10.1002/qj.2788

Scott, R. K., & Polvani, L. M. (2004). Stratospheric control of upward wave flux near the tropopause. *Geophysical Research Letters*, *31*, L02115. https://doi.org/10.1029/2003GL017965

Scott, R. K., & Polvani, L. M. (2006). Internal variability of the winter stratosphere. Part I: Time-independent forcing. *Journal of Atmospheric Sciences*, *63*(11), 2758–2776. https://doi.org/10.1175/JAS3797.1

Seviour, W. J. M., Mitchell, D. M., & Gray, L. J. (2013). A practical method to identify displaced and split stratospheric polar vortex events. *Geophysical Research Letters*, *40*, 5268–5273. https://doi.org/10.1002/grl.50927

Seviour, W. J. M., Waugh, D. W., Polvani, L. M., Correa, G. J. P., & Garfinkel, C. I. (2017). Robustness of the simulated tropospheric response to ozone depletion. *Journal of Climate*, *30*(7), 2577–2585. https://doi.org/10.1175/JCLI-D-16-0817.1

Shaw, T. A., & Perlwitz, J. (2013). The life cycle of Northern Hemisphere downward wave coupling between the stratosphere and troposphere. *Journal of Climate*, *26*(5), 1745–1763. https://doi.org/10.1175/JCLI-D-12-00251.1

Shaw, T. A., & Perlwitz, J. (2014). On the control of the residual circulation and stratospheric temperatures in the Arctic by planetary wave coupling. *Journal of the Atmospheric Sciences*, *71*(1), 195–206. https://doi.org/10.1175/JAS-D-13-0138.1

Sigmond, M., Scinocca, J., Kharin, V., & Shepherd, T. (2013). Enhanced seasonal forecast skill following stratospheric sudden warmings. *Nature Geoscience*, *6*(2), 98–102.

Solomon, S. (1999). Stratospheric ozone depletion: A review of concepts and history. *Reviews of Geophysics*, *37*, 275–316.

Souders, M. B., Colle, B. A., & Chang, E. K. M. (2014a). The climatology and characteristics of Rossby wave packets using a feature-based tracking technique. *Monthly Weather Review*, *142*(10), 3528–3548. https://doi.org/10.1175/MWR-D-13-00371.1

Souders, M. B., Colle, B. A., & Chang, E. K. M. (2014b). A description and evaluation of an automated approach for feature-based tracking of Rossby wave packets. *Monthly Weather Review*, *142*(10), 3505–3527. https://doi.org/10.1175/MWR-D-13-00317.1

Strahan, S. E., Douglass, A. R., & Steenrod, S. D. (2016). Chemical and dynamical impacts of stratospheric sudden warmings on Arctic ozone variability. *Journal of Geophysical Research*, *121*, 11,836–11,851. https://doi.org/10.1002/2016JD025128

Taguchi, M. (2016). Features of vortex split MSSWs that are problematic to forecast. *Atmospheric Science Letters*, *17*(9), 517–522. https://doi.org/10.1002/asl.686

Thompson, D. W. J., Baldwin, M. P., & Wallace, J. M. (2002). Stratospheric connection to Northern Hemisphere wintertime weather: Implications for prediction. *Journal of Climate*, *15*(12), 1421–1428. https://doi.org/10.1175/1520-0442(2002)015<1421:SCTNHW>2.0.CO;2

Tripathi, O. P., Baldwin, M., Charlton-Perez, A., Charron, M., Eckermann, S. D., Gerber, E., . . . Son, S.-W. (2015). The predictability of the extratropical stratosphere on monthly time-scales and its impact on the skill of tropospheric forecasts. *Quarterly Journal of the Royal Meteorological Society*, *141*(689), 987–1003.

Tripathi, O. P., Baldwin, M., Charlton-Perez, A., Charron, M., Cheung, J. C. H., Eckermann, S. D., . . . Stockdale, T. (2016). Examining the predictability of the stratospheric sudden warming of January 2013 using multiple NWP systems. *Monthly Weather Review*, *144*(5), 1935–1960. https://doi.org/10.1175/MWR-D-15-0010.1

Tripathi, O. P., Charlton-Perez, A., Sigmond, M., & Vitart, F. (2015). Enhanced long-range forecast skill in boreal winter following stratospheric strong vortex conditions. *Environmental Research Letters*, *10*(10), 104007.

Trounday, B., Perthuis, L., Strebelle, S., Farrara, J. D., & Mechoso, C. R. (1995). Dispersion properties of the flow in the southern stratosphere during winter and spring. *Journal of Geophysical Research*, *100*(D7), 13,901–13,917. https://doi.org/10.1029/95JD00774

Waugh, D. W. (1997). Elliptical diagnostics of stratospheric polar vortices. *Quarterly Journal of the Royal Meteorological Society*, *123*, 1725–1748.

Waugh, D. W., & Randel, W. J. (1999). Climatology of Arctic and Antarctic polar vortices using elliptical diagnostics. *Journal of Atmospheric Sciences*, *56*, 1594–1613.

World Meteorological Organization (WMO) (2015). Scientific assessment of ozone depletion: 2014 (Global Ozone Research and Monitoring Project WMO Rep. 25). Geneva, Switzerland.

Zhang, J., Tian, W., Chipperfield, M. P., Xie, F., & Huang, J. (2016). Persistent shift of the Arctic polar vortex towards the Eurasian continent in recent decades. *Nature Climate Change*, *6*, 1094–1099. https://doi.org/10.1038/nclimate3136

Honorary Awards and Degrees Committee
New Mexico Tech Faculty Senate

20 April 2018

    We are pleased to nominate the paper "Characterizing stratospheric polar vortex variability with computer vision techniques", by Zachary D. Lawrence and Gloria L. Manney, for the 2018 Langmuir Award. Zac Lawrence, the lead author, is currently finishing his fourth year in the PhD graduate program in Physics at New Mexico Tech. His paper represents a major advance in describing the behavior of stratospheric polar vortices, leading to new insights into the evolution of and impacts of polar vortex disturbances, including the dynamical processes that control the amount of Arctic ozone loss in the Northern Hemisphere winter/spring and how stratospheric polar vortex disturbances can affect weather and climate.

    The paper was submitted to the *Journal of Geophysical Research: Atmospheres* in August of 2017, and was accepted in November with minor revisions after receiving very favorable reviews. The reviewers noted that the paper was "very well written, cited, and organized", the "results are relevant and timely", and that the approach is "superior in a number of respects" to previously used methods, as well as commenting on specific aspects of the study that led to new insights. *JGR: Atmospheres* has an impact factor of 3.45 and is widely considered one of the premier journals for the study of Earth's atmosphere. The paper was published in final form in February 2018, and has already been cited in both papers in press and in submitted manuscripts.

    Zac was awarded a 3-year NASA Earth and Space Science Graduate Fellowship in 2016 to work in this project. His paper is the cornerstone of that effort as well as the foundation for more papers during 2018 that are in progress. Last year, Zac completed and extended his CAVE-ART (Characterization and Analysis of Vortex Evolution using Algorithms for Region Tracking) software for characterizing the stratospheric polar vortices using computer vision techniques. His JGR paper includes a detailed description of CAVE-ART as well as discussing more general methods and considerations for using computer vision techniques in geophysical applications. The methods developed for and described in this paper are already being used for further studies of the stratospheric vortex as well as in independent atmospheric physics studies (e.g., analysis of the Asian summer monsoon anticyclone). Zac developed segmentation, descriptive, and tracking algorithms for CAVE-ART that provide a comprehensive description of the dynamical and geometrical evolution of polar vortices. These methods can characterize and track multiple vortex regions over time and identify vortex disturbances. The paper includes not only a description of the unique way in which he uses computer vision techniques to analyze the stratospheric polar vortex, but also new insights on two important aspects of
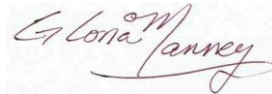
polar vortex dynamics, namely polar vortex splitting events and physically-based measures of polar vortex strength. Using meteorological datasets, Zac identified thirty-eight split-like events in the Arctic vortex between 1980 and 2017.

Zac presented this work at the American Meteorological Society Middle Atmosphere Conference in June 2017, where it was highly praised and received a "Best Student Presentation" Award. He is now using the results from CAVE-ART that were reported in this paper to develop new methods using additional computer vision and machine learning techniques, to explore unique polar vortex signatures that may precede sudden stratospheric warmings ("preconditioning"), and to study how different states of the stratospheric polar vortex may have varying effects on surface weather and climate. The work he described in the nominated paper both provides important new insights on the structure and evolution of the stratosphere polar vortex (which are important to improving weather forecasts and climate models) and also demonstrates innovative new methods that can be applied to numerous analyses of massive datasets in atmospheric physics and other fields. The accompanying letters from researchers in the field provide further insights into the importance and expected impact of Zac's paper.

Sincerely,

Kenneth Minschwaner
Wilkening Professor of Physics
New Mexico Tech

Gloria Manney
Senior Research Scientist
NorthWest Research Associates;
Adjunct Professor of Physics
New Mexico Tech

LABORATOIRE DE MÉTÉOROLOGIE DYNAMIQUE

UMR 8539 - Ecole Polytechnique - Université Paris Saclay
91128 PALAISEAU Cedex (FRANCE)
Secrétariat : +33 (0)1 69 33 51 01   Télécopie : +33 (0)1 69 33 51 08
Site Web : http ://www.lmd.jussieu.fr/

Votre correspondant ; **Peter Hitchcock**
               +33 (1) 69 33 51 51
               peter.hitchcock@lmd.polytechnique.fr

Palaiseau, April 19, 2018

To whom it may concern,

I am writing in support of the nomination of the article 'Characterizing Stratospheric Polar Vortex Variability With Computer Vision Techniques' by Zachary Lawrence and Gloria Manney for the Langmuir Award for an outstanding scientific research paper. This paper has made valuable contributions to the understanding of the variability of the stratospheric polar vortex and should stimulate interesting new research in several areas.

The polar vortex in the Arctic stratosphere exhibits complex, three-dimensional variability. This variability is of global significance for understanding the recovery of the ozone layer in response to the implementation of the Montreal protocol which limited the emission of ozone depleting substances. it is also of substantial interest for the forecasting of surface weather and climate, since in extreme cases, variability of this stratospheric vortex can lead to cold air outbreaks over much of North America and Europe. Predicting these impacts, however, requires a detailed understanding of the mechanisms which drive the variability of the vortex.

This is where this article has made substantial contributions: the techniques adopted from computer vision and applied to dynamical quantities relevant to the stratospheric polar vortex have revealed common patterns of variability in the vortex, and have provided a more precise means of quantifying the winds near the vortex edge. These diagnostics suggest new dynamical questions to investigate, and provide the potential for more accurate comparisons and evaluations of the global models used to understand stratospheric ozone recovery and to predict the surface impacts of stratospheric variability.

In view of these contributions, I am pleased to support the nomination of this article for the Langmuir Award.

Peter Hitchcock

Dr. V. Lynn Harvey
600 UCB, Space Sciences Bldg
3665 Discovery Drive
Boulder, CO 80303-7820
Telephone: (303) 492-2920
Email: lynn.harvey@lasp.colorado.edu

April 17, 2018

To Whom It May Concern:

I am writing to support the nomination of Zachary Lawrence to receive the Langmuir Award for his recent paper published in the Journal of Geophysical Research Atmospheres entitled, *Characterizing stratospheric polar vortex variability with computer vision techniques*. I have been working in the field of stratospheric polar vortex dynamics for the past 26 years and have read many hundreds of peer-reviewed manuscripts on the topic. Given that experience I attest that Mr. Lawrence's paper is perhaps the most comprehensive and creative presentation I have ever read. In addition, the methods he developed are novel, state-of-the art, and innovative. Indeed, the results that he recently published were undocumented heretofore because they required the sophisticated "Characterization and Analysis of Vortex Evolution using Algorithms for Region Tracking (CAVE-ART)" computer vision and image processing techniques that he developed over the past few years as part of the pursuit of his doctoral degree.

It is extremely difficult to tell a computer to track a feature in a fluid that your eye can easily see. It is even more difficult to tell a computer to keep track of multiple "objects" at the same time and to retain information about the shape of those objects and the flow field in which they are moving. However, Zachary accomplished just that with respect to the stratospheric polar vortex. The results presented in the above paper reveal characteristics about the vortex, such as a higher incidence of splitting apart, that call into question previously accepted understanding. Since an ongoing topic of research shows that vortex split behavior effects weather patterns at the surface, Zachary's results have tangible "real world" impacts.

The paper describes and demonstrates the CAVE-ART technique by applying it to study the polar vortex in the stratosphere; however, this new analysis package is versatile and can be used to study coherent vortex structures in, for example, the ocean, in plasma, in the laboratory, and on Jupiter. Overall, it would be more characteristic for the techniques and results presented in the above paper to come from a world recognized fluid dynamics expert. That Zachary is still a graduate student indicates that he is at the beginning of a very productive and fruitful career.

Please feel free to contact me if you need more information.

All the best,

V. Lynn Harvey
Research Scientist
Laboratory for Atmospheric and Space Physics
University of Colorado - Boulder